

THESIS

THE CONTRIBUTION OF CLOUDS TO GLOBAL SURFACE TEMPERATURE  
VARIABILITY ON MONTHLY TO DECADEAL TIMESCALES

Submitted by

Chloe Boehm

Department of Atmospheric Science

In partial fulfillment of the requirements

For the Degree of Master of Science

Colorado State University

Fort Collins, Colorado

Spring 2022

Master's Committee:

Advisor: David W.J. Thompson

David Randall

Daniel McGrath

Copyright by Chloe Boehm 2022

All Rights Reserved

## ABSTRACT

### THE CONTRIBUTION OF CLOUDS TO GLOBAL SURFACE TEMPERATURE VARIABILITY ON MONTHLY TO DECADAL TIMESCALES

Cloud radiative effects (CREs) have well documented impacts on the mean climate, and have recently been found to play a key role in climate variability in the tropics. This thesis expands on previous work to probe the role of CREs on extratropical surface temperature variability. The impact of CREs on climate variability is isolated using the 'cloud-locking' method run on the Max Planck Earth System Model. This method involves comparing the output from two climate simulations: one in which clouds are coupled to the atmospheric circulation, and another in which clouds are prescribed and thus decoupled from the flow. Results show that coupling between CREs and the atmospheric circulation leads to widespread increases in extratropical surface temperature variability, particularly over the North Atlantic and North Pacific.

This work then explores on what timescales surface temperature variability is increased. In general, CREs play an increasingly large role in surface temperature variability at increasingly long timescales. Importantly, cloud-circulation coupling leads to enhanced decadal temperature variability of  $\sim 25\text{--}45\%$  over most of the Northern Hemisphere oceans and  $\sim 10\text{--}15\%$  over most of the land areas. Finally, using a simple expression for temperature variance in terms of the surface energy balance, the mechanisms driving these variability changes are identified. This variability enhancement derives from 'reddening' of surface temperature variability by cloud shortwave radiative effects. These results demonstrate the dominant effect that cloud-circulation coupling has on interannual and decadal temperature variability across much of the globe. This work has implications for the interpretation of observed decadal variability, and for the importance of cloud-circulation coupling in climate model simulations.

## ACKNOWLEDGEMENTS

I would like to thank my advisor, Dr. David W.J. Thompson, for his continual wisdom and guidance on this work and throughout the master's program. I would also like to thank Dr. David Randall and Dr. Daniel McGrath for serving on my committee. Thank you to the past and present members of the Thompson group (Luke Davis, Shim Yook, Lina Boljka, Casey Patrizio, Jingyuan Li, and James Larson) for insightful discussions and advice. Finally, I would like to thank my friends and family for their invaluable inspiration and support, especially my partner Lilly.

## TABLE OF CONTENTS

ABSTRACT . . . . .	ii
ACKNOWLEDGEMENTS . . . . .	iii
LIST OF FIGURES . . . . .	v
Chapter 1      Introduction . . . . .	1
1.1          The Global Energy Budget . . . . .	2
1.2          Cloud Radiative Effect . . . . .	4
1.3          Uncertainty in Global Climate Models . . . . .	6
1.4          COOKIE and Cloud-Locking Methods . . . . .	6
1.5          The Impact of Clouds on Internal Climate Variability . . . . .	8
1.6          Thesis Goals . . . . .	9
Chapter 2      Methods and Data . . . . .	11
2.1          Cloud-Locking Method . . . . .	11
2.2          Observational Dataset . . . . .	12
2.3          Analysis Techniques . . . . .	12
2.3.1      Calculation of Variability . . . . .	12
2.3.2      Time Filtering . . . . .	13
Chapter 3      Results . . . . .	15
3.1          Patterns of Variability . . . . .	15
3.2          Timescales of Surface Temperature Variability . . . . .	22
3.3          Mechanisms Driving Variability Changes . . . . .	34
Chapter 4      Conclusions . . . . .	43
4.1          Implications . . . . .	43
4.2          Connection to Observations . . . . .	44
4.3          Future Work . . . . .	45
References . . . . .	48
Appendix A    Surface Temperature Variance Decomposition . . . . .	54

## LIST OF FIGURES

1.1	Reproduced, from Fig. 4.1 of Hartmann (2016). A schematic of terms of the surface energy balance. Net radiation ( $R_s$ ); latent heat ( $LE$ ); sensible heat ( $SH$ ); heat storage below the surface ( $\partial E_s/\partial t$ ); horizontal energy flux below the surface ( $\Delta F_{eo}$ ). . . . .	3
1.2	Reproduced, from Fig. 7.7 of Boucher et al. (2013). Annual-mean top of atmosphere (a) shortwave, (b) longwave, and (c) net cloud radiative effects. . . . .	5
3.1	Standard deviation of monthly-mean surface temperature anomalies for (a,d) the 200-year interactive simulation and (b,e) the 200-year locked simulation. (c,f) The fractional changes in standard deviations between simulations. Note that the colorscale is different in the two rows. . . . .	16
3.2	The fractional change in standard deviation of monthly-mean temperature anomalies between the interactive and locked simulation at (a,b) 200 hPa, (c,d) 500 hPa, (e,f) the surface (same at Fig.3.1 c,f) . . . . .	18
3.3	Standard deviation of monthly-mean anomalous geopotential height for (a,d,g) the 200-year interactive simulation and (b,e,h) the 200-year locked simulation. (c,f,i) The fractional changes in standard deviations between simulations. Results are shown for three levels of the atmosphere: (a,b,c) 200 hPa, (d,e,f) 500 hPa, and (g,h,i) the surface. . . . .	20
3.4	Standard deviation of monthly-mean anomalous zonal wind for (a,d,g) the 200-year interactive simulation and (b,e,h) the 200-year locked simulation. (c,f,i) The fractional changes in standard deviations between simulations. Results are shown for three levels of the atmosphere: (a,b,c) 200 hPa, (d,e,f) 500 hPa, and (g,h,i) the surface. . . . .	21
3.5	The fractional changes in surface temperature standard deviation between the locked-cloud and interactive simulations. (a,b) Temperatures are unfiltered (same as Fig.3.1c,f). (c,d) Temperatures have been one-year low-pass filtered. (e,f) Temperatures have been one-year high pass filtered. . . . .	24
3.6	The fractional changes in surface temperature standard deviation between the locked-cloud and interactive simulations. (a,b) Temperatures have been one-year low-pass filtered. (c,d) Temperatures have been three-year low-pass filtered. (e,f) Temperatures have been ten-year low-pass filtered. . . . .	25
3.7	Changes in surface temperature variability for five different Northern Hemisphere regions due to cloud-circulation coupling. (a,b) Fractional changes in Northern Hemisphere ( $15^\circ$ - $90^\circ$ N) three-year low-pass temperature variability reproduced from Fig. 3.6. Fractional changes in standard deviation of surface temperature for different low-pass filter lengths and averaged over (c) entire Arctic ( $60^\circ$ - $90^\circ$ N), (d) North Pacific ( $15^\circ$ - $60^\circ$ N, $129^\circ$ - $241^\circ$ E), (e) North America ( $15^\circ$ - $60^\circ$ N, $196^\circ$ - $305^\circ$ E), (f) North Atlantic ( $15^\circ$ - $60^\circ$ N, $285^\circ$ - $360^\circ$ E), (g) Eurasia ( $15^\circ$ - $60^\circ$ N, $0^\circ$ - $170^\circ$ E). . . . .	27

3.8	Changes in surface temperature variability for two different Southern Hemisphere regions due to cloud-circulation coupling. (a,b) Fractional changes in Southern Hemisphere (30°-90°S) three-year low-pass temperature variability reproduced from Fig. 3.6. Fractional changes in standard deviation of surface temperature for different low-pass filter lengths and averaged over (c) Southern Ocean (30°-60°S) and (d) entire Antarctic (60°-90°S) . . . . .	29
3.9	Area-averaged monthly-mean time series of surface temperature anomalies for the interactive and locked-cloud simulations over (a,b) all ocean areas and (c,d) all land areas. Grayed lines show unfiltered time series, blue and orange lines indicate three-year (a,c) and ten-year (b,d) low-pass filtered time series for the interactive and locked-cloud simulations respectively. The time series for the locked-cloud simulation is offset by 1.5K for ocean areas and 2.5K for land areas to distinguish the time series. . . . .	30
3.10	Area-averaged monthly-mean time series of surface temperature anomalies for the interactive and locked-cloud simulations over (a) North America, (b) the North Pacific, (c) the entire Arctic, (d) the North Atlantic, (e) the entire Antarctic, (f) the Southern Ocean, (g) Eurasia, and (h) the entire Tropics (15°S-15°N). Extratropical regions are defined in the caption of Figures 3.7 and 3.8. Grayed lines show unfiltered time series, blue and orange lines indicate three-year low-pass filtered time series for the interactive and locked-cloud simulations, respectively. The time series for the locked-cloud simulation is offset by 7K for land areas, and 1.25K for ocean areas to distinguish the two time series. . . . .	32
3.11	Same as Fig. 3.10 except for with ten-year low-pass filtered time series for the interactive (blue line) and locked-cloud (orange line) overlaid on top of unfiltered time series (grayed line). . . . .	33
3.12	The ratio of surface temperature variance from the interactive simulation to the locked-cloud simulation for (a) surface temperature variance values from each simulation, and (b) calculated surface temperature variance for each simulation using variance decomposition equation (Eq. 3.3) . . . . .	36
3.13	(a-c) The ratio of each term on the right-hand side of Eq. 3.3 calculated for the interactive and locked simulation. (d) Each term on the right-hand side of Eq. 3.3 multiplied together to recreate the surface temperature variance ratio between the interactive and locked simulation. . . . .	38
3.14	Surface energy flux variances: (a,b) surface shortwave radiative flux, (c,d) surface longwave radiative flux, (e,f) surface sensible heat flux, (g,h) surface latent heat. The left column shows the variance for the interactive-cloud simulation. The right column shows the contribution of each individual flux variance to the total surface flux variance of the interactive simulation. . . . .	39
3.15	Surface energy flux variances for the interactive simulation (left column), locked-cloud simulation (middle column), and the fractional change in variance between the two simulations (right column). (a-c) Surface shortwave radiative flux, (d-f) surface longwave radiative flux, (g-i) surface sensible heat flux, and (j-l) surface latent heat flux. . . . .	41

4.1 Surface energy flux variances: (a,b) surface shortwave radiative flux, (c,d) surface longwave radiative flux, (e,f) surface sensible heat flux, (g,h) surface latent heat flux. The left column shows the individual flux variances for the interactive simulation. The right column shows the individual flux variances as estimated by ERA5 reanalysis. . . 46

# Chapter 1

## Introduction

One of the most pressing issues of our time is constraining future projections of the climate under anthropogenic warming. Clouds and their radiative effects give rise to some of the most important – and most uncertain – feedbacks under climate change (e.g. Bony & Dufresne, 2005; Bony et al., 2015; Sherwood et al., 2020; Zelinka & Hartmann, 2010, and references therein). This makes the study of clouds and their radiative effects critical to better predictions of the future climate. It has also been well established that clouds play an essential role in the mean climate and in the dynamical response to climate change (e.g. Albern et al., 2018; Albern et al., 2019; Albern et al., 2020; Ceppi & Hartmann, 2015, 2016; Grise et al., 2019; Stephens et al., 2012; Voigt & Albern, 2019; Voigt et al., 2021; Voigt & Shaw, 2015, 2016, and references therein). In recent years, it has become clear that clouds play an important role in climate variability (e.g. Li et al., 2020; Middlemas et al., 2019; Rädcl et al., 2016). A complicating factor in future climate projections is the role of internal climate variability, providing additional motivation to further our understanding of clouds in this context.

The role of clouds in climate variability has been investigated primarily in the tropics (e.g. Li et al., 2020; Middlemas et al., 2019; Rädcl et al., 2016). Cloud radiative effects (CREs) have proven important for simulated variability in the El-Niño/Southern Oscillation (Middlemas et al., 2019; Rädcl et al., 2016) and for tropics-wide variations in the sea-surface temperature field (Li et al., 2020). However, the importance of CREs for extratropical variability is generally less clear, and most studies have focused on the importance of CREs for relatively short-term variability (Grise et al., 2019; Li et al., 2014; Papavasileiou et al., 2020; Schäfer & Voigt, 2018). Longer-term variability patterns play a key role in modulating warming patterns due to climate change, so they are equally as important to fully understand (Cassou et al., 2018).

The goal of this thesis is to evaluate the role that CREs play in simulated extratropical surface temperature variability. In addition, we will explore the timescales on which CREs have an effect

on extratropical temperature variability, with a focus on low-frequency variability. Thirdly, this work will investigate the mechanisms behind the impact of CREs on extratropical temperature variability, in order to develop a full understanding of the variability changes. The results of this work have potentially important implications for the interpretation of observed and predicted extratropical temperature variability changes.

In this chapter, Sections 1.1 and 1.2 review relevant background of the global energy budget and the cloud radiative effect. Section 1.3 concerns the uncertainty in global climate models as it relates clouds. Section 1.4 discusses current methodology and relevant past work on the impact of clouds within the climate. Section 1.5 furthers this discussion by reviewing recent studies on the role of clouds in climate variability. Motivation and an outline of this thesis is then provided in section 1.6.

## **1.1 The Global Energy Budget**

Earth's energy budget describes the flow of energy in and out of the climate system. Understanding Earth's energy budget and its individual components allows us to better understand the dynamics of the climate and predict how it will change under climate change (Forster et al., 2021). At the top of the atmosphere (TOA), the energy budget is comprised of incoming shortwave radiation and outgoing longwave radiation. In equilibrium these two terms balance each other; however, due to internal climate variability and anthropogenic forcing, an imbalance can occur resulting in excess heating or cooling. Similar to the energy balance at the TOA, the surface energy balance can be described as the balance of net shortwave and longwave radiative flux but with the addition of non-radiative components such as latent, sensible, and horizontal heat fluxes of the land-ocean surface (see Fig. 1.1, Hartmann, 2016). Changes in the surface energy balance drive atmosphere and ocean dynamics and are of particular importance due to the practical significance of understanding changes in surface climate.

A description of the Earth's energy budget is not complete without the inclusion of clouds which are essential regulators of Earth's energy fluxes. Incoming solar shortwave radiation is

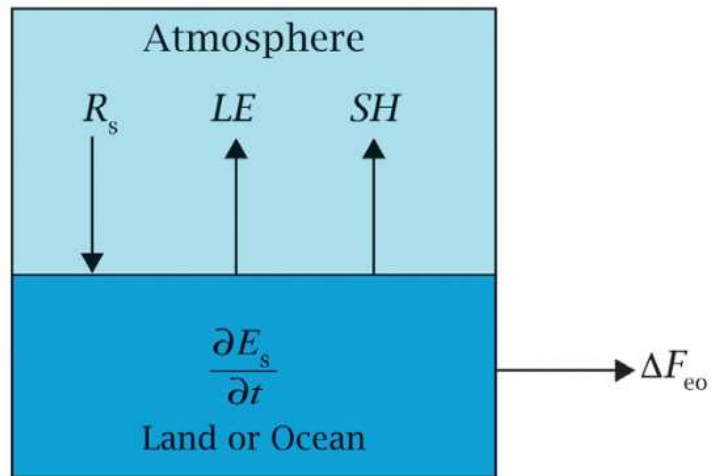


**Figure 1.1:** Reproduced, from Fig. 4.1 of Hartmann (2016). A schematic of terms of the surface energy balance. Net radiation ( $R_s$ ); latent heat ( $LE$ ); sensible heat ( $SH$ ); heat storage below the surface ( $\partial E_s/\partial t$ ); horizontal energy flux below the surface ( $\Delta F_{eo}$ ).

reflected by clouds, increasing the planetary albedo and cooling the planet. At the same time, longwave radiation emitted by Earth's surface is absorbed and reemitted at cooler temperatures by clouds, warming the planet (Ramanathan et al., 1989). In the net, these competing effects act to ultimately warm or cool the planet, varying regionally and temporally.

## 1.2 Cloud Radiative Effect

The cloud radiative effect (CRE) describes the net effect of clouds on the global energy budget. Ramanathan (1987) first quantified the CRE as the difference between clear-sky and cloudy-sky radiative fluxes at the TOA. The net CRE can be broken down into two components - the shortwave CRE and the longwave CRE. The shortwave CRE is the effect of clouds on the shortwave radiation while the longwave CRE is the effect of clouds on the longwave radiation. Satellite observations have been used for decades to measure the radiative fluxes at the TOA which then were used to calculate the CRE (e.g. Loeb et al., 2018; Ramanathan, 1987; Ramanathan et al., 1989; Stephens et al., 2012). Initial studies showed that the shortwave CRE is generally negative and the longwave CRE is generally positive but as advances in satellite observations occurred, studies were able to show the significant regional differences in the shortwave CRE, longwave CRE, and net CRE (see Fig. 1.2, Boucher et al., 2013).

Regional differences and additional temporal differences can be attributed to differing cloud properties and amount of incoming shortwave radiation. Fig. 1.2a shows that areas such as the tropics, Southern Ocean, North Atlantic, and North Pacific have the strongest shortwave CRE. These are all regions with optically thick clouds that are thus more effective at reflecting incoming shortwave radiation. Polar regions have a weaker shortwave CRE due to the lack of available sunlight. Fig. 1.2b illustrates a similar point for the longwave CRE - regions with high clouds where the radiating temperature is cold have the strongest longwave CRE compared to regions with primarily low clouds. The net CRE is the addition of the shortwave CRE and longwave CRE and can be seen in Fig. 1.2c. Since the negative shortwave CRE outweighs the positive longwave

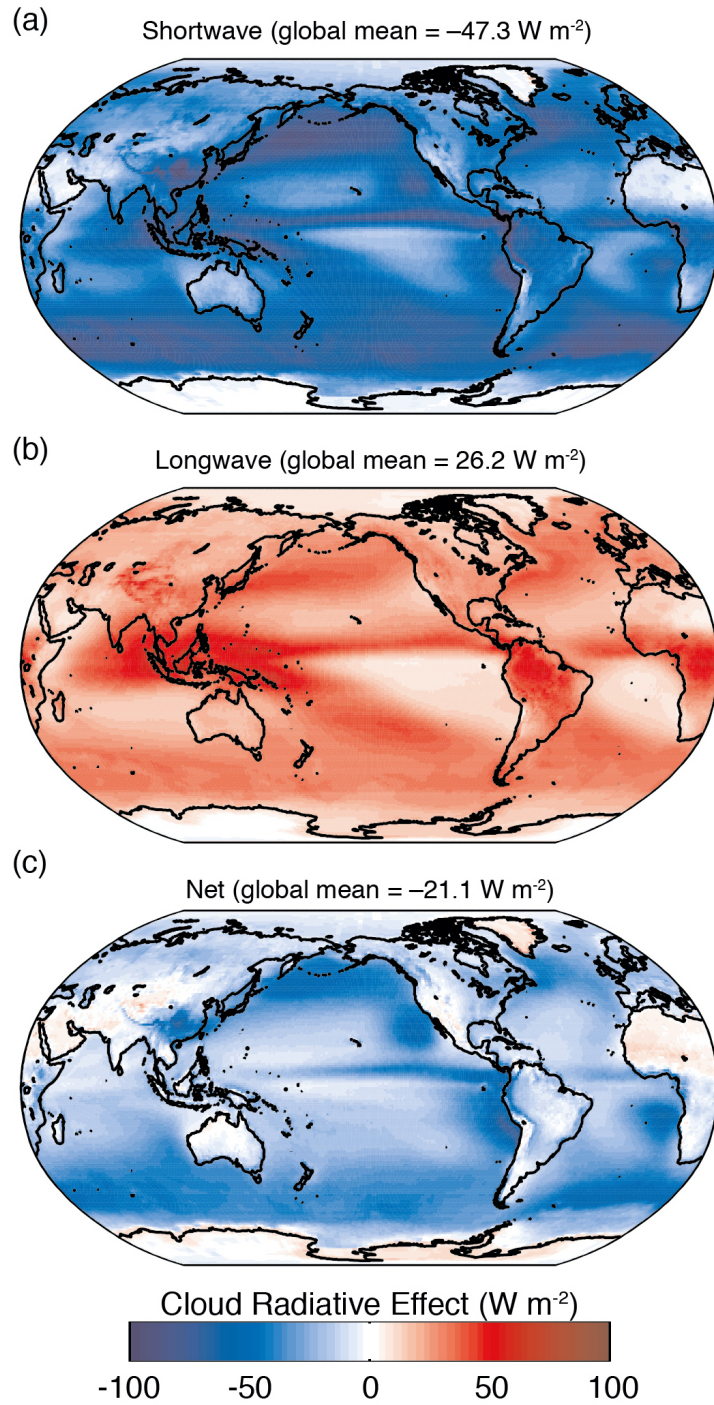


**Figure 1.2:** Reproduced, from Fig. 7.7 of Boucher et al. (2013). Annual-mean top of atmosphere (a) shortwave, (b) longwave, and (c) net cloud radiative effects.

CRE, the net CRE is negative across most of the globe. Regional differences are again apparent due to differing properties of clouds and the strength of the resulting shortwave and longwave CRE.

A global-mean net CRE of about  $-21 \text{ Wm}^{-2}$  (see Fig. 1.2c) illustrates the importance of clouds in the climate system and that without them, the climate would warm significantly. In comparison, the radiative forcing resulting from a doubling of  $\text{CO}_2$  is only about  $4 \text{ Wm}^{-2}$  (Zelinka & Hartmann, 2010). Thus, it is essential to consider how clouds and their radiative effects will change with climate change and the potential implications this has on other aspects of the climate system.

### **1.3 Uncertainty in Global Climate Models**

Despite the importance of evaluating CREs in the context of climate change, cloud feedbacks remain the largest source of uncertainty in global climate model estimates (Bony et al., 2006; Bony & Dufresne, 2005; Sherwood et al., 2020; Zelinka & Hartmann, 2010, and references therein). Part of the challenge to constraining cloud feedbacks is that global climate models are not cloud process resolving and thus parameterizations must be used. The multitude of cloud properties and formation processes are very difficult to accurately represent and only a small change in one aspect of a cloud can have a dramatic effect on the climate (Sherwood et al., 2020).

Another aspect of global climate models that remains uncertain is the influence of clouds on the atmospheric circulation. The connection between clouds and the circulation has substantial impacts on 1) the mean state of the present-day circulation and climate, 2) the circulation response to climate change, and 3) the internal variability of the circulation (Voigt et al., 2021). These impacts have been primarily investigated using two prominent methods – Clouds On-Off Climate Model Intercomparison Experiment and cloud-locking.

### **1.4 COOKIE and Cloud-Locking Methods**

There are two methods that have gained prominence recently for isolating the cloud radiative impact on atmospheric circulation: Clouds On-Off Climate Model Intercomparison Experiment (COOKIE, Stevens et al., 2012) and cloud-locking.

The COOKIE method involves comparing two experiments - a control simulation where clouds are fully coupled and include CREs ('cloud-on' experiment) and a 'cloud-off' experiment where clouds are transparent to the radiation and thus CREs are turned off. The cloud-off experiment still simulates the other impacts clouds have such as precipitation and latent heating (Stevens et al., 2012). Comparing these two experiments isolates the impact of CREs on the model climate. Since in the cloud-off experiment there is no cloud radiative heating or cooling, the atmospheric circulation is altered. So, COOKIE is useful for studying the impact of the presence of clouds on the mean circulation, but is not useful in the context of climate change and climate variability (Voigt & Albern, 2019).

Despite its limitations, COOKIE has been used for decades in numerous studies to illustrate the large impact of CREs on the large-scale mean circulation (Albern et al., 2018; Hunt, 1978; Li et al., 2015; Slingo & Slingo, 1988). Hunt (1978) and Albern et al. (2018) both explored the notable impact of clouds on the position and strength of the mean tropical circulation while Slingo and Slingo (1988) and Li et al. (2015) considered the role of cloud radiative interactions in the midlatitude and polar circulations, finding that the substantial effect of clouds extends outside of the tropics.

Since COOKIE is only useful for exploring the mean climate, the cloud-locking method was developed as a more suitable way for exploring impacts of CREs in the context of climate change and climate variability (Voigt et al., 2021). The cloud-locking method involves comparing two simulations – one where clouds are fully coupled to the atmospheric circulation ('interactive' simulation) and one where clouds are prescribed and thus decoupled from the circulation ('locked-cloud' simulation). In the locked-cloud simulation, the mean climate and circulation are preserved which allows the contribution of CRE changes to climate variability and response to climate change to be explored (Voigt et al., 2021, and references therein).

Cloud-locking has been used extensively to show the meaningful impact CREs have on the dynamical response to climate change (e.g. Ceppi & Hartmann, 2015, 2016; Voigt & Albern, 2019; Voigt et al., 2021, and references therein). Specifically, these studies established that under

climate change, clouds impact the shift of extratropical jet streams and storm tracks (Albern et al., 2019; Grise et al., 2019; Voigt & Shaw, 2015, 2016). In fact, Ceppi and Hartmann (2016) found that CREs cause more than half of the total shift of the midlatitude jet stream and storm tracks and the Hadley cell under climate change. Additionally, it was found that tropical cloud radiative changes dominate global circulation changes when compared to midlatitude and polar cloud radiative changes (Albern et al., 2019).

In addition to understanding how the impact of CREs on the current climate and circulation under climate change, in order to reduce uncertainty in climate model projections, it is critical to understand the role of internal variability (Deser et al., 2012). In particular, the role of clouds and their radiative effects on internal climate variability is an active area of research with many aspects still unknown (Voigt et al., 2021).

## **1.5 The Impact of Clouds on Internal Climate Variability**

In recent years, it has become clear that clouds play an important role in climate variability with much of this recent work focused on the impact of clouds in the tropics (e.g. Li et al., 2020; Middlemas et al., 2019; Rädel et al., 2016). CREs have been proven important for simulated variability in the El-Niño/Southern Oscillation (ENSO) although there is some disagreement on the timescales and mechanisms of these variability changes (Middlemas et al., 2019; Rädel et al., 2016). Middlemas et al. (2019) found that ENSO variability was only increased on timescales shorter than 6 years due to a damping shortwave CRE on longer timescales, while Rädel et al. (2016) found that ENSO variability was increased across all timescales due to a positive longwave CRE. Part of these differences could be attributed to the fact that these two studies used different cloud-locking methodologies and different models.

Li et al. (2020) extended this work by looking at tropics-wide variations in the sea-surface temperature field. Coupling between atmospheric circulation and clouds increased sea-surface temperature variability across the tropical oceans on monthly to decadal timescales due to the ‘reddening’ of shortwave CREs. As such, shortwave CREs increased variability on low-frequency

timescales (e.g. timescales longer than a few days) but decreased variability on high-frequency timescales (e.g. timescales of a few hours).

The importance of CREs for extratropical variability is generally less clear, most studies have focused on the importance of CREs for relatively short-term dynamic variability (Grise et al., 2019; Li et al., 2014; Papavasileiou et al., 2020; Schäfer & Voigt, 2018). However, understanding the role of CREs on extratropical climate variability on longer timescales is equally important as better insight into the mechanisms of interannual to decadal variability can help to improve climate prediction skill.

Extratropical oceans exhibit considerable decadal variability (Deser & Blackmon, 1993; Deser & Phillips, 2017), but the mechanisms behind this variability is still not fully understood (Wills et al., 2021). Oceans play a large role in regulating the variability of the rest of the climate due to their large heat capacity and ability to communicate energy changes with the atmosphere via radiative and turbulent heat fluxes (Deser et al., 2010). This makes understanding the mechanisms behind this variability critical. Surface heat fluxes and ocean currents are cited as primary mechanisms (Årthun et al., 2021; Deser et al., 2010) while minimal research has been done about the role of clouds. Since previous work has shown the substantial impact of clouds on tropical sea-surface temperature variability on low-frequency timescales (Li et al., 2020), it is necessary to see if clouds also have a similar impact in the extratropical regions. Additionally, investigating the influence of clouds on patterns of low-frequency variability over land areas has not been well examined but is of considerable practical significance for understanding future surface temperature variability patterns.

## **1.6 Thesis Goals**

As summarized in prior sections, previous research has shown the pronounced impact of clouds on climate variability, as well as the implications of this impact in the context of climate change. Specifically, recent work has shown that clouds notably impact climate variability in the tropical oceans (Li et al., 2020; Middlemas et al., 2019; Rädel et al., 2016). The overarching goal of this

thesis is to further this past work by demonstrating that CREs play a fundamental role in climate variability not only in the tropics, but also in the extratropics. This is accomplished using the cloud-locking method described briefly in section 1.4 and described in more detail in Chapter 2. Due to the practical significance of understanding surface temperature variability, this thesis will primarily explore the impacts of CREs on this aspect of the climate system. In addition to exploring generally how CREs impact surface temperature variability, this work will investigate on what timescales surface temperature variability is changed due to CREs. Furthermore, the mechanisms behind variability changes will be investigated using a simple expression for the temperature variance in terms of changes in the surface energy budget.

Chapter 2 discusses the cloud-locking method, the data that was used in this work, and the additional analysis methods performed. Chapter 3 highlights the results of exploring the impact of clouds on surface temperature variability in extratropical regions using the cloud-locking method. Finally, Chapter 4 discusses key findings and provides a direction for future research.

# Chapter 2

## Methods and Data

This section will detail the cloud-locking simulations, additional data that was used in this work, and analysis techniques, namely, how changes in variability were represented and time filtering that was performed on the data.

### 2.1 Cloud-Locking Method

In order to perform our analysis, we used output from two simulations run on a fully-coupled Earth System Model. The first was an “interactive” or control simulation where cloud radiative effects (CREs) are fully coupled to the atmospheric circulation, and the second was a “locked” simulation where CREs are decoupled from the flow. Both simulations were run by D. Olonscheck on the Max Planck Institute Earth System Model at low resolution (MPI-ESM1.2-LR, Mauritsen et al., 2019). These simulations are identical to the ones used in Li et al. (2020).

The MPI-ESM1.2-LR model has T63 ( $\sim 200$  km) horizontal resolution and 47 vertical levels in the atmosphere, and  $1.5^\circ$  ( $\sim 150$  km) horizontal resolution with 40 vertical levels in the ocean. The interactive simulation was run for 250 years with preindustrial forcing but only the last 200 years of the simulation were used to account for model spin-up. The locked simulation was performed in the same way, except that all cloud parameters were randomized before being read into the radiation code. This was achieved by first saving cloud parameters from the interactive simulation at every two-hour radiation call. Then, the order of the years were shuffled but not the hours or days associated with the cloud properties at each timestep. Lastly, these shuffled cloud parameters were read into the radiation code at each two hour timestep for the whole model run. Thus, the cloud parameters in the locked simulation maintained the same long-term mean diurnal and seasonal cycles as those in the interactive simulation, but they are decoupled from variability in the atmospheric circulation on all timescales. This allowed us to isolate the impact of cloud-circulation coupling and thus CREs on climate variability. For more details on the locking methodology see Rädcl et al.

(2016), Olonscheck et al. (2019), and Li et al. (2020); for details on the experiments used here see Li et al. (2020).

The output from these simulations was monthly-mean data for a variety of variables, of which temperature, individual surface energy fluxes, geopotential height, and zonal wind were used for this work. The data was detrended by removing the linear trend and then anomalies of the monthly-mean data were created by subtracting the mean value of each month across all years. As noted above, the output is the same as was used in the recent study Li et al. (2020). In that work, they focused on the tropics and did not identify large changes in surface temperature variability in the extratropical regions. This was, in part, because they did not explore results for the extratropics in depth or consider temperature variability in those regions on low-frequency timescales. For this study, we focus on the extratropics in both the Northern and Southern Hemisphere.

## **2.2 Observational Dataset**

In order to determine if results from the cloud-locking simulations were applicable to the real-world, we compared the variance of the surface fluxes from the interactive simulation to the variance of the observed fluxes, as estimated by ECMWF ERA5 reanalysis (Hersbach et al., 2020). ERA5 is a global reanalysis that combines observations with models to create a globally complete map of a large number of atmospheric, oceanic, and land climate variables. It has a horizontal resolution of 30km and 137 vertical levels in the atmosphere. ERA5 data was obtained in monthly-mean format from the ECMWF data server for the January, 1979 – July, 2021 time period. The variables used were surface latent heat flux, surface shortwave radiation, surface longwave radiation, and surface sensible heat flux.

## **2.3 Analysis Techniques**

### **2.3.1 Calculation of Variability**

First, we explored the changes in surface temperature, geopotential height, and zonal wind variability between the locked and interactive simulations. To do this, the standard deviation of

each variable was calculated for each simulation. This computation was done by determining the anomalous monthly-mean sample variance and then taking the square root to get the sample standard deviation. The sample variance is defined as:

$$\overline{x'^2} = \frac{1}{N-1} \sum_{i=1}^N (x_i - \bar{x})^2, \quad (2.1)$$

where  $\bar{x}$  is the sample mean,  $x_i$  is an individual sample,  $N$  is the number of samples, the subscript  $i$  denotes the time step, and primes denote departures from the mean. The sample standard deviation is thus then defined as

$$s = \sqrt{\overline{x'^2}}. \quad (2.2)$$

Changes in the variability are shown as the fractional change in standard deviation:

$$\frac{s_i}{s_l} - 1, \quad (2.3)$$

where  $s_i$  and  $s_l$  denote the standard deviation for the interactive and locked simulations, respectively. Next, the variance of each individual surface energy flux was calculated using Eq. 2.1 to explore changes in the variances between simulations. This was used to diagnose the mechanisms behind changes in temperature variability using a derived expression for the temperature variance. This expression and details on its derivation can be found in Chapter 3 and Appendix A.

### 2.3.2 Time Filtering

In part of this thesis, the timescales of variability change were explored. The technique to isolate the variability on certain frequencies was time filtering. This time filtering was done by employing a Butterworth filter. A Butterworth filter is a recursive filter that is designed to be smooth, have a flat frequency in the passband, and have high tangency at the origin and infinity. This filter was run as a low-pass filter on the temperature data multiple times with different cutoff frequencies to see how variability patterns changed as the filter length changed.

Besides the cutoff frequency, the order of filter also needed to be specified. The higher the order the sharper the cutoff but a high order also means that more data points must be discarded on the ends. Due to the nature of the filter, some of the data points in the beginning and end will be corrupted before the response starts to settle out. Thus, it is necessary to balance the order of the filter and the amount of data that must be discarded as a result. To determine how much data must be discarded, we plotted the impulse response function and determined the number of timesteps it took for the function to become negligible.

We determined that an order of seven was the best balance with the amount of data that must be discarded. Based on the impulse response function, the number of data points that would need to be discarded at both ends of the dataset was equal to half of the filter length. For example, when the filter was run with a length of 60 months, the first and last 30 months of dataset were removed.

# Chapter 3

## Results

The goal of this chapter is to detail the results of our investigation into the role of clouds in climate variability. First, spatial maps of temperature, geopotential height, and zonal wind variability are shown for multiple levels of the atmosphere and for both the interactive and locked simulations. Variability patterns for each variable are compared between the two simulations by calculating the fractional change in standard deviation as detailed in section 2.3.1. Next, we explored the timescales on which these variability changes occurred. Specifically, we focused on extratropical surface temperature variability changes on low-frequency timescales using time filtering as this has not been well explored in previous work. Lastly, we asked the question: why does cloud-circulation coupling lead to increased variability in extratropical surface temperatures? Following previous work by Yu and Boer (2006) and Li et al. (2020), a simple expression is derived to explain the mechanisms that contribute to the temperature variance from the surface energy balance. This allows us to evaluate which mechanisms act to enhance or dampen surface temperature variability as a result of cloud-circulation coupling.

### 3.1 Patterns of Variability

Figures 3.1-3.2 explore the differences in temperature variability between the interactive simulation – where clouds are coupled to the climate system, and the locked simulation – where clouds are decoupled from the circulation. The climatological standard deviations of surface temperature from the interactive and locked runs are shown in the left and middle columns of Fig. 3.1, respectively. Results for the ocean areas are shown in the top row; results for land areas are shown in the bottom row. Land areas have generally more surface temperature variability than ocean regions due to the low heat capacity of land compared to the ocean. In both simulations, the land areas with the largest standard deviations are found over Northern Hemisphere (NH) midlatitude regions, the Arctic, and the Antarctic. Over the oceans, the temperature variance is most pronounced in the

### Standard Deviation of Surface Temperature

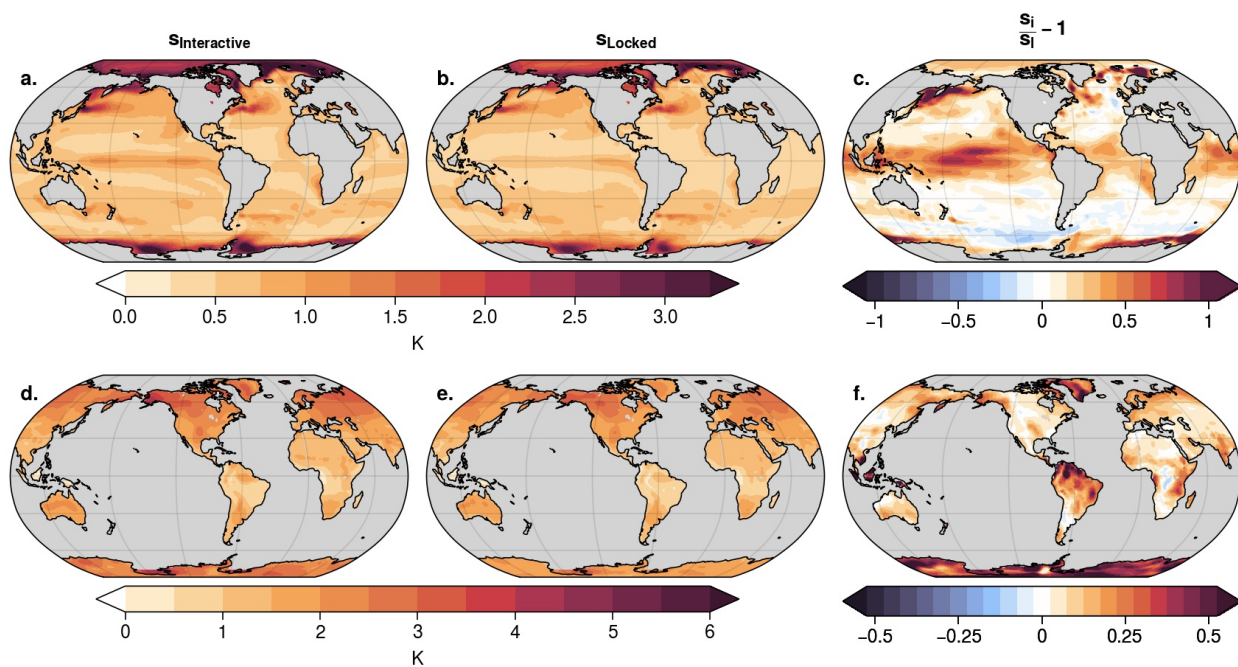


**Figure 3.1:** Standard deviation of monthly-mean surface temperature anomalies for (a,d) the 200-year interactive simulation and (b,e) the 200-year locked simulation. (c,f) The fractional changes in standard deviations between simulations. Note that the colorscale is different in the two rows.

Gulf Stream and Kuroshio Current regions, locations where ocean heat transport is particularly important.

The fractional changes in the standard deviations ( $\frac{s_i}{s_l} - 1$ ) are shown in the right column of Fig. 3.1. The numeric values of these fractional changes can be interpreted as a percent increase or decrease in surface temperature variability due to cloud-circulation coupling. For example, a value of 0.5 would indicate there is a 50% increase in the variability of surface temperature when clouds are coupled to the circulation. Alternatively, a value of  $-0.5$  would indicate a 50% decrease in variability in the interactive simulation.

Coupling between cloud radiative effects (CREs) and the atmospheric circulation leads to widespread increases in surface temperature variability over the North Pacific, Tropics, Arctic, Antarctic, and most land areas (Fig. 3.1 panels c and f). It also leads to increases over much of the North Atlantic with the exception of select regions over the center of the basin. The Southern Ocean is an exception to this general trend where CREs do not have a distinct influence on surface temperature variability. In fact, there are regions that exhibit a decrease in surface temperature variability due to cloud-circulation coupling.

Widespread increases in temperature variability due to CREs also extends throughout the atmosphere. Fig. 3.2 illustrates the fractional change in temperature standard deviation for three different levels of the atmosphere: the surface, 500 hPa, and 200 hPa. Surface temperature variability in Fig. 3.2e,f is reproduced from Fig. 3.1c,f. Results for ocean areas are shown separately from results for land areas, each with a different colorscale. Across the tropics, temperature variability is increased by upwards of 40–50% across the land and ocean. Notable increases in variability appear throughout the rest of the globe but to a slightly lesser extent. Although cloud-circulation coupling generally impacts temperature variability similarly across all levels, the regional differences in the impact of CREs apparent at the surface (Fig. 3.2 e,f), do not extend to the higher levels of the atmosphere. This is expected partially because of the differing cloud types present at each atmospheric level and thus resulting differences in the cloud radiative effect. Additionally, hori-

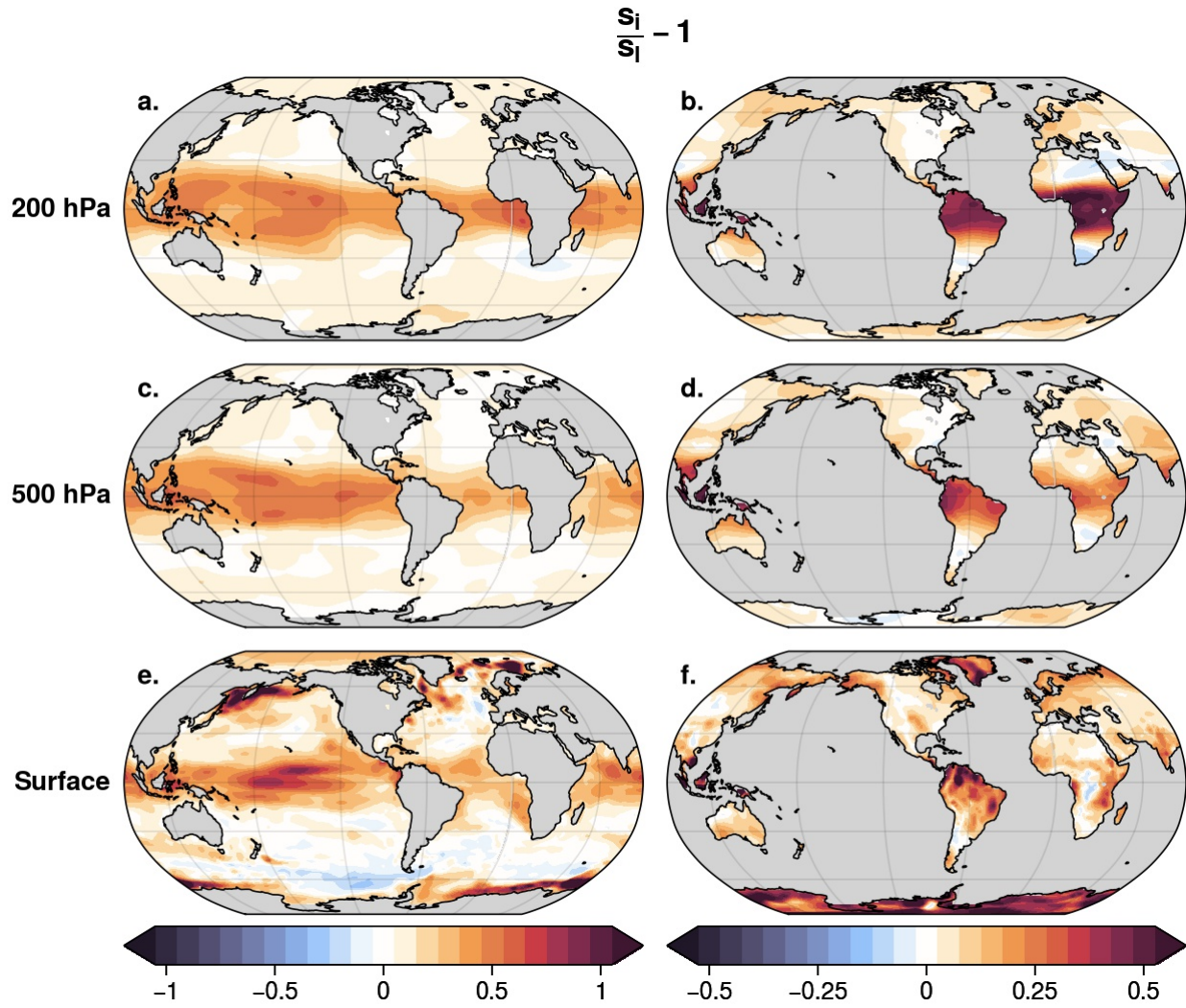


**Figure 3.2:** The fractional change in standard deviation of monthly-mean temperature anomalies between the interactive and locked simulation at (a,b) 200 hPa, (c,d) 500 hPa, (e,f) the surface (same at Fig.3.1 c,f)

zonal heat transport, topography, and other surface level processes are not present which affects temperature variability as a whole.

In an effort to further explore the role of clouds on climate variability, Figures 3.3 and 3.4 show the differences in geopotential height and zonal wind variability between the interactive and locked simulations. Changes in geopotential height variability are shown in Fig. 3.3 to discern how the variability of pressure is changing between simulations while taking into account altitude and latitude differences across the globe.

Geopotential height variability is illustrated for the same three levels of the atmosphere as Fig. 3.2: the surface, 500 hPa, and 200 hPa. Because the land and ocean exhibit a similar magnitude of standard deviation for geopotential height, they are shown on the same plot unlike Fig. 3.2. In both simulations, the standard deviation of geopotential height is largest over high latitudes and increases going from the surface to upper levels of the atmosphere. While the amplitude of variability changes, the variability patterns remain the same between atmospheric levels. The fractional changes in geopotential height standard deviations shown in the right column indicating that cloud-circulation coupling primarily impacts geopotential height variability across the tropics. At the surface and 500 hPa, cloud-circulation coupling slightly increases the variability in the middle and high-latitudes while the variability across the tropics is substantially enhanced. At 200 hPa, the dominant changes in variability due to CREs occur in the tropics. This figure shows that geopotential height variability is primarily enhanced due to CREs at upper levels of the atmosphere and in the tropics.

Similar to Fig. 3.3, Fig. 3.4 shows the role of clouds on climate variability for three levels of the atmosphere for a different climate variable: zonal wind. Exploring the variability of zonal wind between simulations is of interest because of the intimate connection with other aspects of large-scale atmospheric dynamics and resulting transport of energy across the globe. It is clear that for both simulations, the standard deviation of zonal wind increases with atmospheric height, and is similar to the geopotential height, with the largest values in middle to high-latitudes. This can be explained by the location of the jet streams as well as the fact that large temperature variations lead

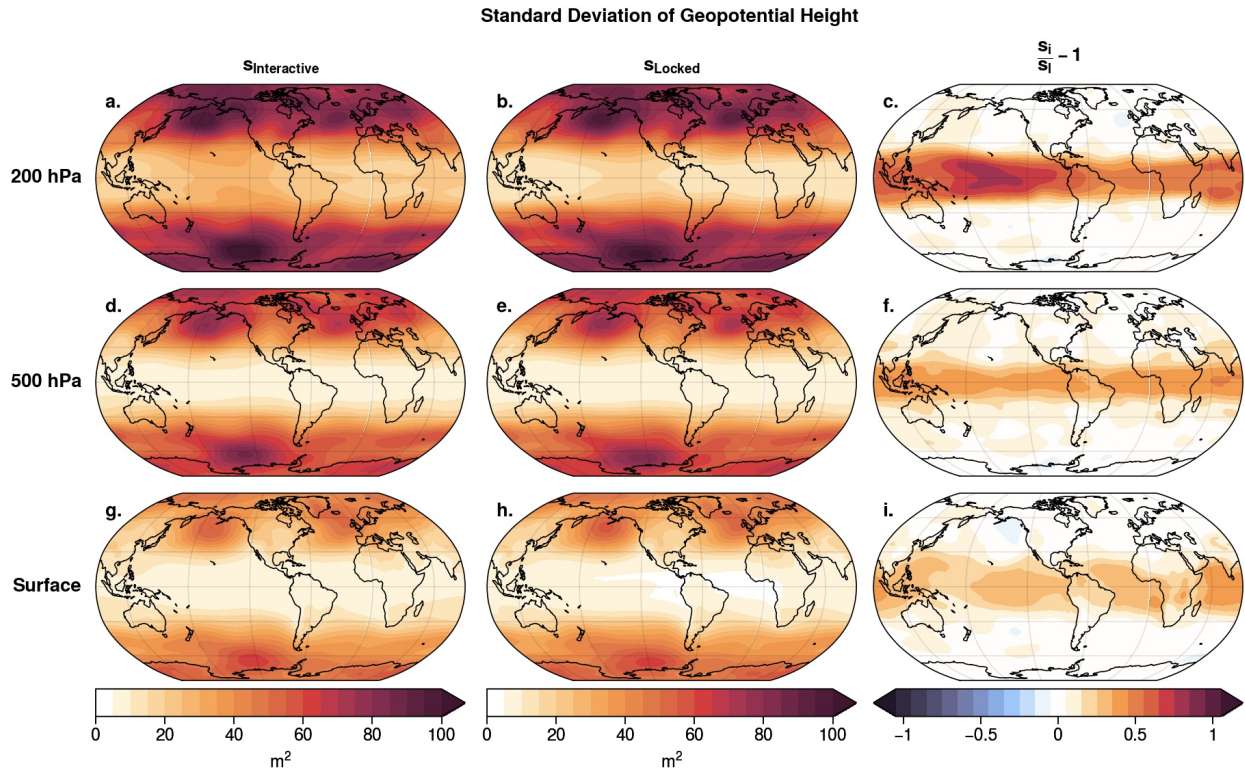


**Figure 3.3:** Standard deviation of monthly-mean anomalous geopotential height for (a,d,g) the 200-year interactive simulation and (b,e,h) the 200-year locked simulation. (c,f,i) The fractional changes in standard deviations between simulations. Results are shown for three levels of the atmosphere: (a,b,c) 200 hPa, (d,e,f) 500 hPa, and (g,h,i) the surface.

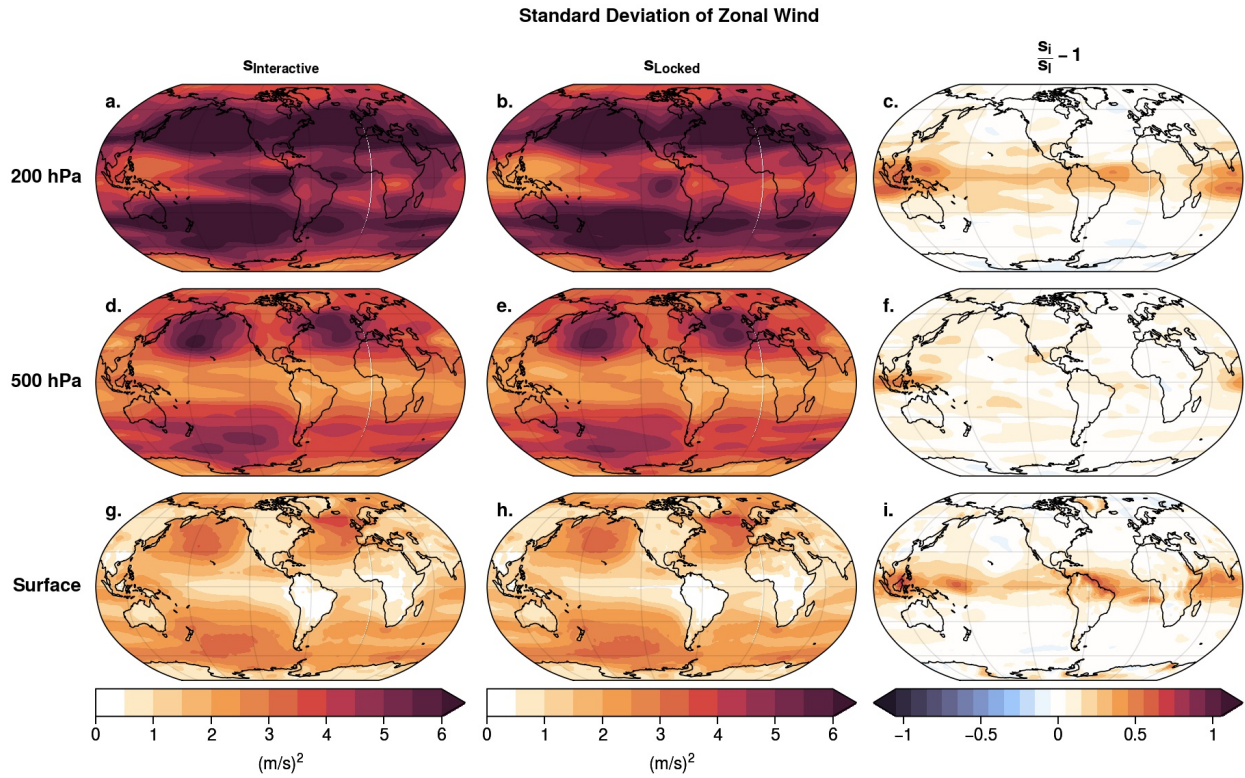


**Figure 3.4:** Standard deviation of monthly-mean anomalous zonal wind for (a,d,g) the 200-year interactive simulation and (b,e,h) the 200-year locked simulation. (c,f,i) The fractional changes in standard deviations between simulations. Results are shown for three levels of the atmosphere: (a,b,c) 200 hPa, (d,e,f) 500 hPa, and (g,h,i) the surface.

to larger zonal winds. Particular areas of interest are the North Atlantic and North Pacific, where zonal wind has substantial variability in both simulations across all levels of the atmosphere.

The right-column of Fig. 3.4 explores which regions experience a change in zonal wind standard deviation as a result of CREs. At both 200 hPa and the surface, the primary region where cloud-circulation coupling influences the variability is in the tropics. This influence is less notable at the 500 hPa level but still present. In general, it is clear from this figure that cloud-circulation coupling has a more pronounced effect on temperature and geopotential height variability than zonal wind variability.

This section, through results in Figures 3.1 – 3.4, has shown the dominant impact cloud-circulation coupling has on multiple aspects of climate variability. Of the climate variables explored, cloud-circulation coupling had the most influence on the extratropical surface temperature variability and thus, the remainder of this work will be focused on exploring this connection further.

## **3.2 Timescales of Surface Temperature Variability**

To further our understanding on the role of clouds, we explored on what timescales CREs impact surface temperature variability. Previous studies on the importance of CREs for extratropical variability primarily focused on short-term dynamic variability with less work exploring longer timescales (e.g. Grise et al., 2019; Li et al., 2014; Papavasileiou et al., 2020; Schäfer & Voigt, 2018). As such, low-frequency variability was a focus of this work, using low-pass time filtering to isolate said variability.

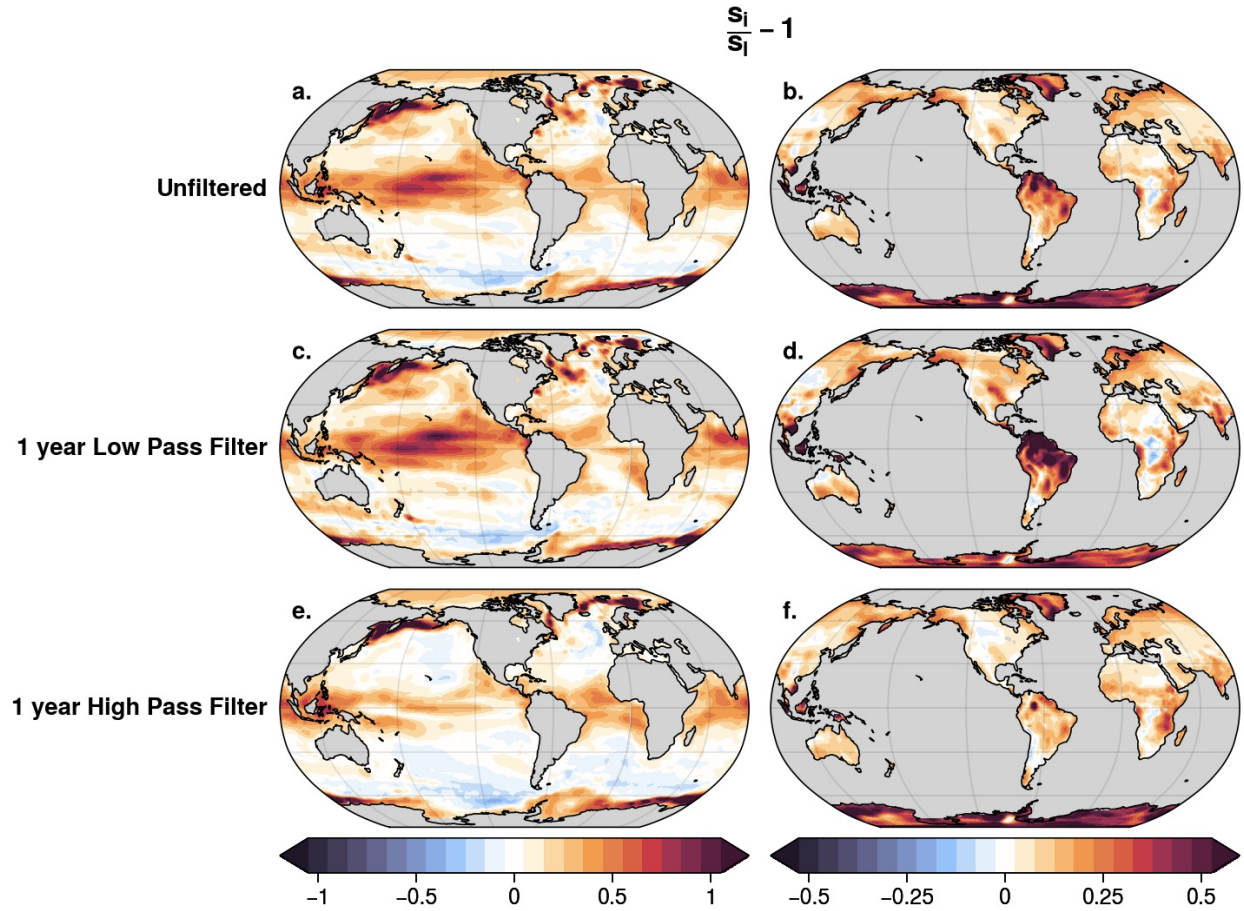
A Butterworth low-pass filter was applied to the surface temperature output of both simulations with multiple filter lengths at six month increments, ranging from six months to ten years. This isolates surface temperature variability that occurs only on timescales greater than the filter length. Initially, we looked at the one-year low-pass filter results compared to the unfiltered temperature data and one-year high-pass filtered data. Fig. 3.5 shows the results of this investigation, illustrating the fractional changes in standard deviation between the interactive and locked simulations for

the unfiltered surface temperature data, the one-year low-pass filtered data, and one-year high-pass filtered data. The high-pass filtered data was calculated by subtracting the low-pass filtered data from the unfiltered data. This isolated only the surface temperature variability on timescales less than one year.

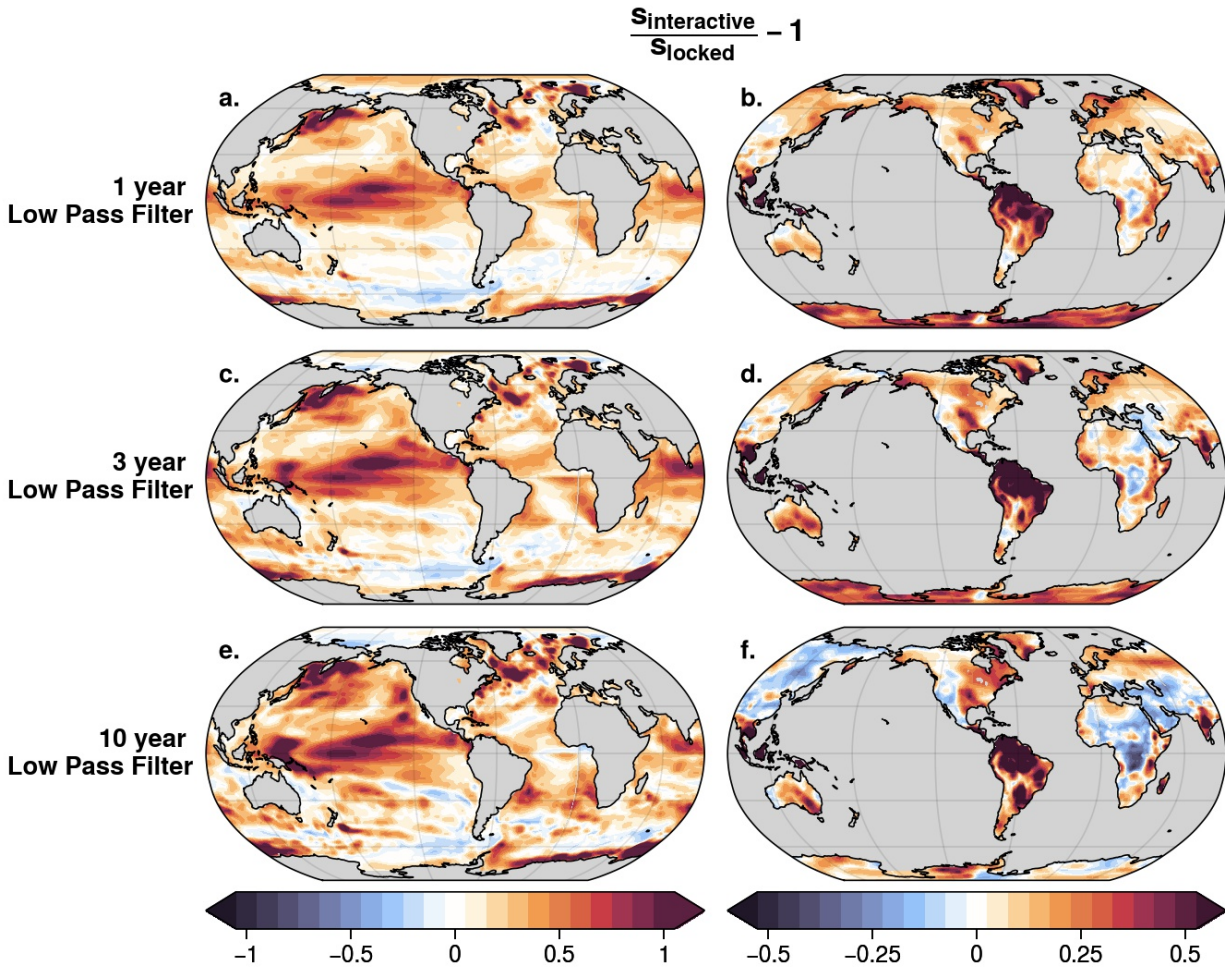
As shown in Fig. 3.5, increases in surface temperature variability are more pronounced on low-frequency timescales than high-frequency timescales. Note that the colorscales are again different in the left and right columns. In certain areas, the variability is increased by upwards of 80–100% over the ocean and 40–50% over land areas. The amplitude of high-frequency temperature variability is smaller and illustrates that CREs have less of an impact on monthly to annual timescales. One exception to this pattern is Antarctic temperature variability. Over the Antarctic, cloud-circulation coupling has a slightly greater impact on timescales less than one year (panel f) compared to longer timescales (panel d). However, it is still important to note that cloud-circulation coupling has a notable impact on Antarctic surface temperature variability on low-frequency timescales.

Fig. 3.6 extends this line of investigation, specifying further the timescales that cloud-circulation coupling has the most impact. Results show the fractional changes in surface temperature variability between simulations for temperatures that have been one, three, and ten-year low-pass filtered. Note again that the colorscales are different for the left and right columns.

In general, cloud-circulation coupling plays an increasingly large role in surface temperature variability at increasingly long timescales. For example, looking at the tropical oceans, North Atlantic, and North Pacific regions in the left panels of Fig. 3.6, it is clear that each of these regions has the most surface temperature variability on decadal timescales or longer. Specifically, cloud-circulation coupling leads to increased extratropical multiannual variability of  $\sim 25\text{--}45\%$  over most of the Northern Hemisphere oceans. In the Southern Hemisphere, there is less of a dramatic change. Certain areas of the Southern Ocean see increasing temperature variability on multiannual to decadal timescales while in other regions, cloud-circulation coupling has a roughly consistent impact across timescales. Interestingly, the variability enhancement due to CREs in the Antarctic appears to decrease as the filter length increases.



**Figure 3.5:** The fractional changes in surface temperature standard deviation between the locked-cloud and interactive simulations. (a,b) Temperatures are unfiltered (same as Fig.3.1c,f). (c,d) Temperatures have been one-year low-pass filtered. (e,f) Temperatures have been one-year high pass filtered.



**Figure 3.6:** The fractional changes in surface temperature standard deviation between the locked-cloud and interactive simulations. (a,b) Temperatures have been one-year low-pass filtered. (c,d) Temperatures have been three-year low-pass filtered. (e,f) Temperatures have been ten-year low-pass filtered.

In the right column of Fig. 3.6, a similar pattern is apparent over land, where cloud-circulation coupling has an increasingly large role in variability at increasingly long timescales. However, there are a few notable areas that do not follow this trend, particularly on decadal timescales. In many parts of Eurasia, Africa, and the western half of North America, CREs play a smaller role in surface temperature variability at decadal timescales. The role of CREs on variability between annual and multiannual timescales remains constant, but on decadal or longer timescales, cloud-circulation coupling acts to *decrease* surface temperature variability in these regions.

The increases in temperature variability due to cloud-circulation coupling are also readily apparent in temperature data averaged over large spatial regions. In order to explore the extratropical regional variations, Figures 3.7 and 3.8 only show the Northern and Southern Hemispheres, respectively, outside of the tropics.

The center panel in Fig. 3.7 reproduces the Northern Hemisphere fractional changes in three-year low-pass temperature variability from Fig. 3.6. The surrounding panels show the changes in standard deviations for temperatures that have been low-pass filtered and averaged over large spatial regions. The low-pass filter length is given on the abscissa of each panel, and the regions are defined in the caption. For example: results at four years on the North Pacific panel indicate the fractional changes in temperature variability for output that has been 1) spatially-averaged over the North Pacific and then 2) four-year low-pass filtered. Cloud-circulation coupling leads to increases in area-mean temperature variability over all Northern Hemisphere regions and for all low-pass filters. The increases are  $\sim 10\text{--}20\%$  over many land areas, approach  $\sim 25\%$  over the North Atlantic, and reach nearly  $\sim 45\%$  over the North Pacific sector. CREs have the most impact on multiannual to decadal timescales in the North Atlantic, North Pacific, and North American regions. Across Eurasia, CREs have roughly equal impacts across all timescales and across the Arctic, the impact of CREs decreases on multiannual to decadal timescales.

Fig. 3.8 shows the same results but for the Southern Hemisphere. The center panel in Fig. 3.8 reproduces the fractional changes in Southern Hemisphere three-year low-pass temperature from Fig. 3.6, and the surrounding panels show the changes in the standard deviations for temperatures

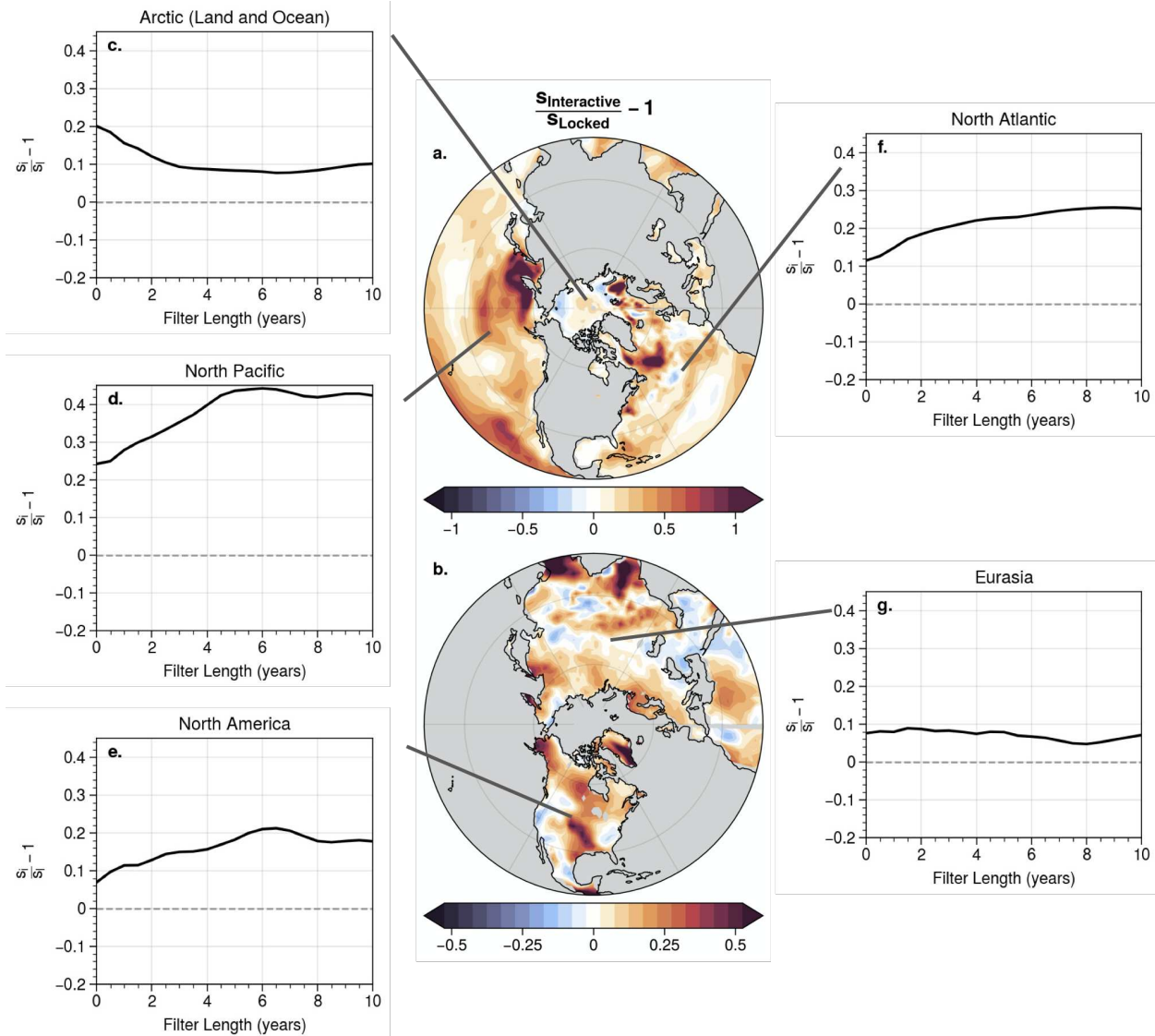


**Figure 3.7:** Changes in surface temperature variability for five different Northern Hemisphere regions due to cloud-circulation coupling. (a,b) Fractional changes in Northern Hemisphere ( $15^{\circ}$ - $90^{\circ}$ N) three-year low-pass temperature variability reproduced from Fig. 3.6. Fractional changes in standard deviation of surface temperature for different low-pass filter lengths and averaged over (c) entire Arctic ( $60^{\circ}$ - $90^{\circ}$ N), (d) North Pacific ( $15^{\circ}$ - $60^{\circ}$ N,  $129^{\circ}$ - $241^{\circ}$ E), (e) North America ( $15^{\circ}$ - $60^{\circ}$ N,  $196^{\circ}$ - $305^{\circ}$ E), (f) North Atlantic ( $15^{\circ}$ - $60^{\circ}$ N,  $285^{\circ}$ - $360^{\circ}$ E), (g) Eurasia ( $15^{\circ}$ - $60^{\circ}$ N,  $0^{\circ}$ - $170^{\circ}$ E).

that have been low-pass filtered and averaged over large spatial regions. Like the Northern Hemisphere, cloud-circulation coupling leads to increases in area-mean temperature variability across the Southern Hemisphere and across all low-pass filters. Temperature variance is increased the most on multiannual to decadal timescales across the Southern Ocean, while over the Antarctic, CREs have a decreasingly important role in temperature variability at increasing timescales.

Together, the results in Figures 3.1-3.8 indicate that cloud-circulation coupling contributes to surface temperature variability over much of the extratropics. The indication that these increases extend to low-frequency timescales has potentially important implications for the interpretation of decadal climate variability. The changes in variability are not only apparent in the changes in standard deviations (Figures 3.1-3.8), but also in the time series of temperature.

For example, Fig. 3.9 shows the time series of simulated temperature variability averaged across all ocean areas (Fig. 3.9 a,b) and all land areas (Fig. 3.9 c,d). Ocean and land areas are shown separately because of the different amplitudes in temperature variability. In addition to the unfiltered time series of surface temperature for each simulation, three or ten-year low-pass filtered time series are overlaid on top.

It is clear from the time series that land areas exhibit more temperature variability than ocean areas, as is expected from the dramatically different heat capacities. Additionally, it is visually apparent that the interactive simulation time series (blue lines) has more variability than the locked simulation time series (orange lines). This is easier to see in the three-year low-pass filtered time series than the ten-year low-pass filtered time series. This could be due to the large regional differences in variability shown in Figures 3.7 and 3.8, and thus it was important to look at regionally averaged time series.

Figures 3.10 and 3.11 show the time series of simulated temperature variability over each of the land and ocean regions shown in Figures 3.7 and 3.8 in addition to the tropics. Even though the focus of this work is the extratropics, it was interesting to see how extratropical temperature variability changes compared to variability changes between the simulations in the tropics.

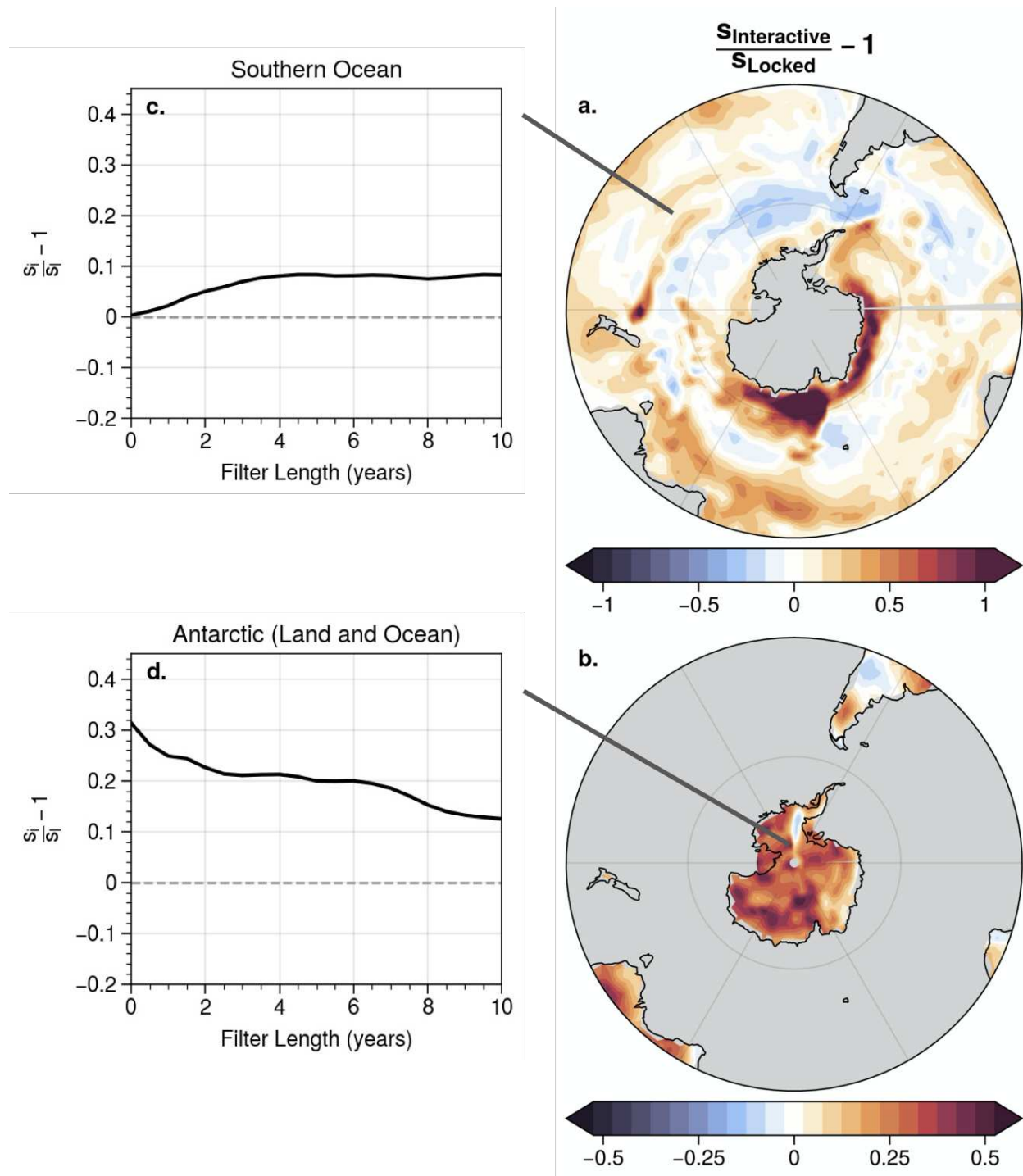


**Figure 3.8:** Changes in surface temperature variability for two different Southern Hemisphere regions due to cloud-circulation coupling. (a,b) Fractional changes in Southern Hemisphere (30°-90°S) three-year low-pass temperature variability reproduced from Fig. 3.6. Fractional changes in standard deviation of surface temperature for different low-pass filter lengths and averaged over (c) Southern Ocean (30°-60°S) and (d) entire Antarctic (60°-90°S)

### Global Mean Unfiltered Time Series and Low Pass Filtered Time Series

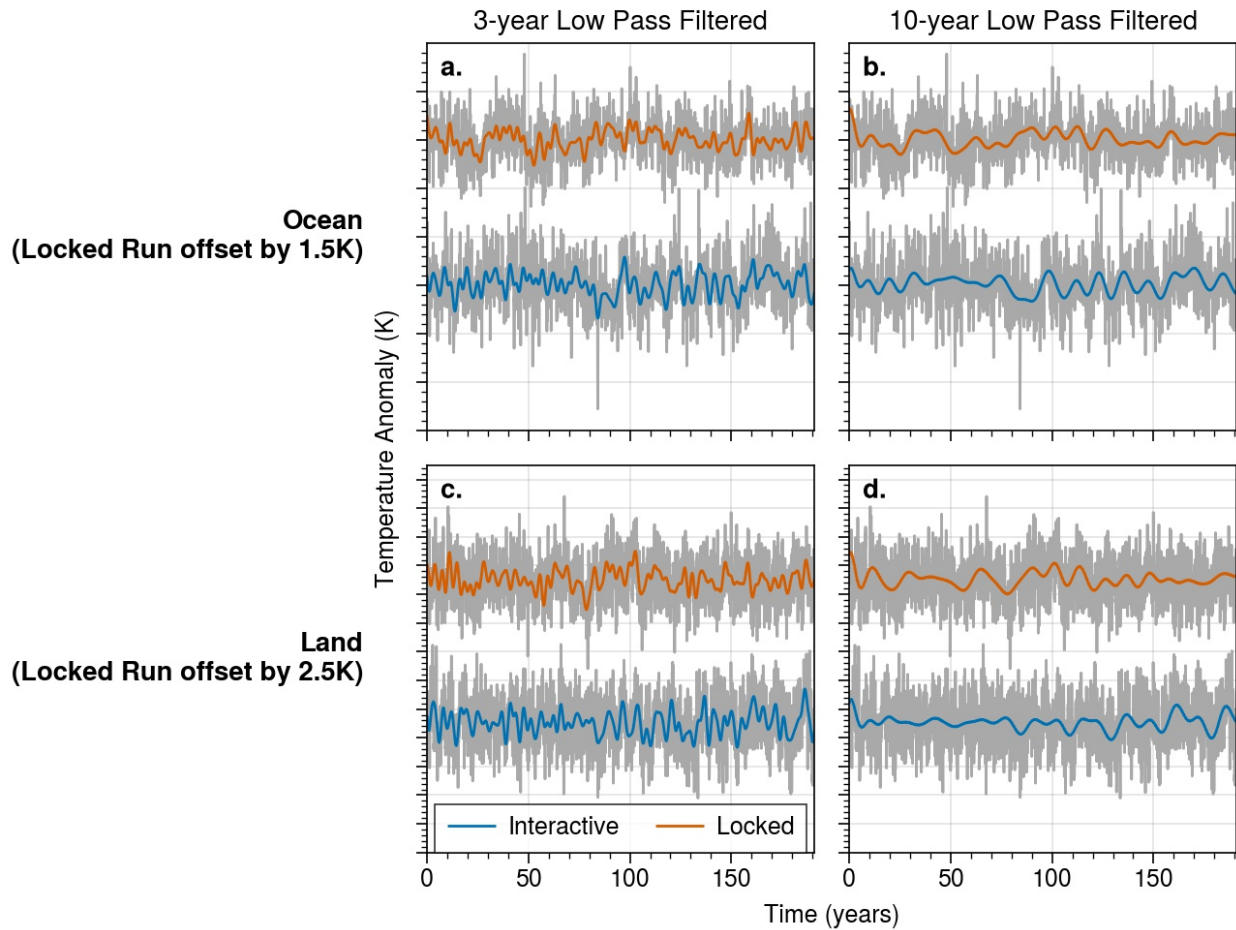


**Figure 3.9:** Area-averaged monthly-mean time series of surface temperature anomalies for the interactive and locked-cloud simulations over (a,b) all ocean areas and (c,d) all land areas. Grayed lines show unfiltered time series, blue and orange lines indicate three-year (a,c) and ten-year (b,d) low-pass filtered time series for the interactive and locked-cloud simulations respectively. The time series for the locked-cloud simulation is offset by 1.5K for ocean areas and 2.5K for land areas to distinguish the time series.

Unfiltered surface temperature time series compared to three-year low-pass filtered time series for each region is shown in Fig. 3.10. Here, the differences in temperature variability between the two simulations are more clear. The North Pacific, North Atlantic, Tropics, and North American regions have a clear visual increase in variability between the locked simulation and the interactive simulation. Looking at the three-year low-pass filtered time series, it is particularly clear there are multiannual shifts in temperature that are apparent in the interactive simulation and not in the locked simulation. The time series of Eurasia, the Southern Ocean, and both polar regions do not have a clear difference between simulations. Even though, from Figures 3.7 and 3.8, results showed that cloud-circulation coupling acts to increase temperature variability in these regions, it is not visually clear in these time series.

Similar results are shown in Fig. 3.11 but instead of three-year low-pass filtered time series, ten-year low-pass filtered time series are shown. These results illustrate variability differences on decadal timescales versus multiannual timescales. North America, the North Pacific, the North Atlantic, and the tropics once again have the largest visual differences between the simulations. In these regions surface temperatures in the interactive simulation exhibit multiple examples of large shifts on decadal timescales that are not apparent in the locked simulation. Time series of the Arctic, Antarctic, Eurasia, and Southern Ocean regions have less of a change in decadal variability. One can see some temperature shifts on decadal timescales but not to the same extent as the other regions. This is consistent with findings from Figures 3.7 and 3.8.

This section, through results shown in Figures 3.5 – 3.11, illustrates that cloud-circulation coupling has a pronounced effect on multiannual to decadal surface temperature variability, particularly across the North Pacific, North Atlantic, and North American regions. Results have explored the regional differences in the impact of CREs on temperature variability, indicating that while all extratropical regions show an enhancement in area-averaged surface temperature variability due to CREs, the North Atlantic and North Pacific show the largest increase in variability. Cloud-circulation coupling increases the variance of multiannual to decadal sea-surface temperature (SST) variability over the North Atlantic and North Pacific basins by  $\sim 25\%$  and  $\sim 45\%$ ,

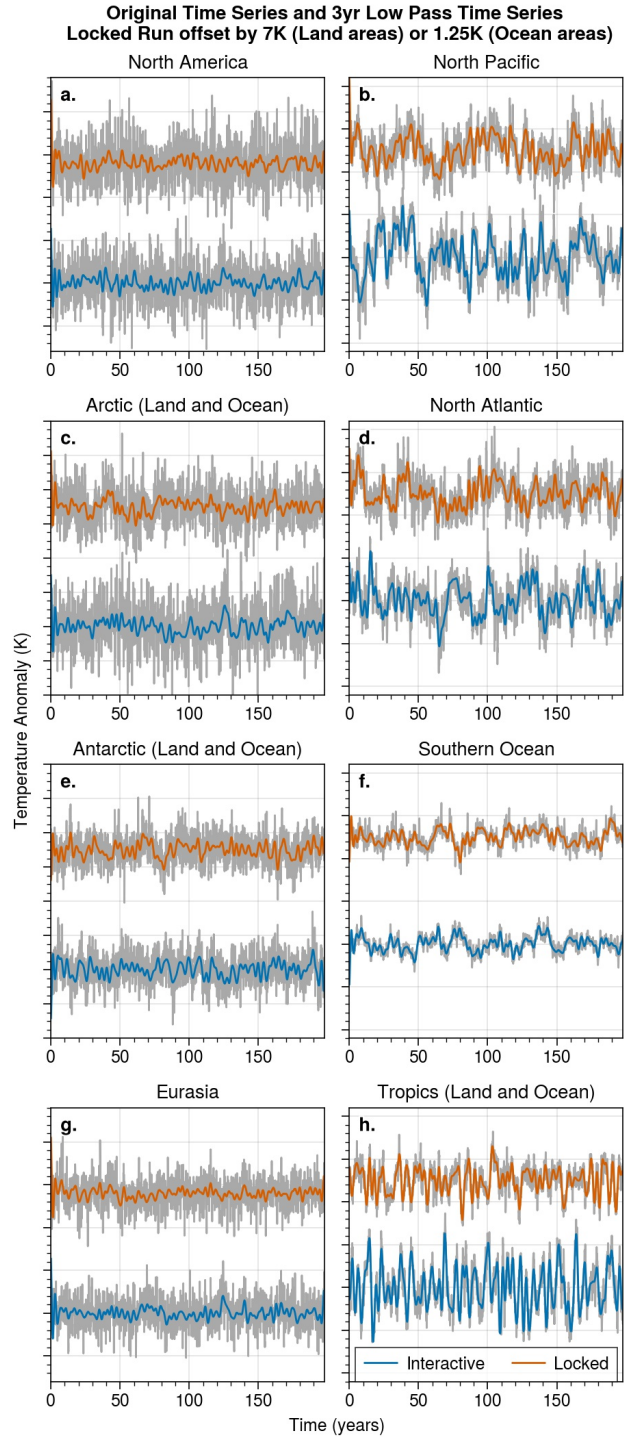


**Figure 3.10:** Area-averaged monthly-mean time series of surface temperature anomalies for the interactive and locked-cloud simulations over (a) North America, (b) the North Pacific, (c) the entire Arctic, (d) the North Atlantic, (e) the entire Antarctic, (f) the Southern Ocean, (g) Eurasia, and (h) the entire Tropics ( $15^{\circ}\text{S}$ - $15^{\circ}\text{N}$ ). Extratropical regions are defined in the caption of Figures 3.7 and 3.8. Grayed lines show unfiltered time series, blue and orange lines indicate three-year low-pass filtered time series for the interactive and locked-cloud simulations, respectively. The time series for the locked-cloud simulation is offset by 7K for land areas, and 1.25K for ocean areas to distinguish the two time series.

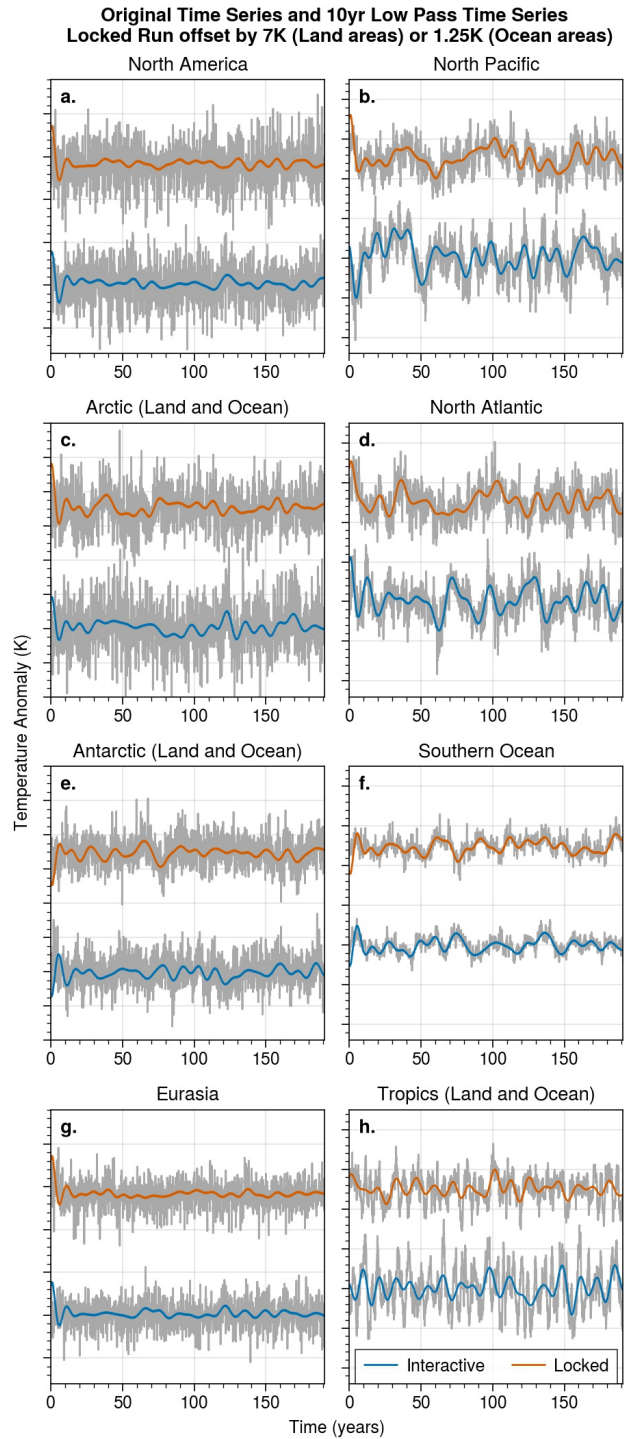


**Figure 3.11:** Same as Fig. 3.10 except for with ten-year low-pass filtered time series for the interactive (blue line) and locked-cloud (orange line) overlaid on top of unfiltered time series (grayed line).

respectively. Our results so far have shown where and on what timescales cloud-circulation has an impact on surface temperature variability. Next, we will explore the mechanisms behind this increased variability.

### 3.3 Mechanisms Driving Variability Changes

Why does cloud-circulation coupling lead to increased variability in extratropical surface temperatures? Following Yu and Boer (2006) and Li et al. (2020), the mechanisms that contribute to the temperature variance can be quantified from the surface energy budget. Starting with the thermodynamic energy equation at the surface:

$$C \frac{dT}{dt} = Q_{SW} + Q_{LW} + Q_{SH} + Q_{LH}, \quad (3.1)$$

where  $C$  is the effective heat capacity of the ocean mixed layer or land surface,  $T$  is the surface temperature, and the  $Q$  terms denote the fluxes of shortwave radiation, longwave radiation, sensible heat, and latent heat, respectively. The conversion of Eq. 3.1 into a diagnostic equation for the temperature variance involves 1) assuming all parameters in Eq. 3.1 reflect departures from the long-term mean; 2) replacing the derivative on the LHS with a centered differencing scheme; 3) squaring the resulting equation and taking the time average (see Li et al., 2020, and Appendix A for details of the procedure). The resulting expression for the temperature variance can be expressed as:

$$\sigma_T^2 = \frac{2(\Delta t)^2}{C^2(1-r_2)} \left( \sigma_\Sigma^2 + 2 \sum \text{cov}(Q_i, Q_j) \right) \quad (3.2)$$

where  $\sigma_T^2$  is the surface temperature variance,  $r_2$  is the lag-2 autocorrelation of temperature,  $\Delta t$  is the sampling timescale (1 month),  $\sigma_\Sigma^2 = \sigma_{SW}^2 + \sigma_{LW}^2 + \sigma_{LH}^2 + \sigma_{SH}^2$  is the sum of the individual surface flux variances, and  $\sum \text{cov}(Q_i, Q_j) = \text{cov}(Q_{SW}, Q_{LW}) + \text{cov}(Q_{SW}, Q_{LH}) + \text{cov}(Q_{SW} + Q_{SH}) + \dots$  is the sum of the covariances between each surface flux term.

This equation can be simplified to:

$$\sigma_T^2 = G\sigma_\Sigma^2 e \quad (3.3)$$

by defining

$$G = \frac{2(\Delta t)^2}{C^2(1-r_2)} \quad (3.4)$$

and

$$e = 1 + \frac{2\Sigma\text{cov}(Q_i, Q_j)}{\sigma_\Sigma^2}. \quad (3.5)$$

$G$  is a ‘transfer term’ that accounts for the influence of persistence (as measured by the lag-two month autocorrelation  $r_2$ ).  $e$  is an ‘efficiency term’ that accounts for the covariances between the various surface fluxes (i.e. negative correlations between different fluxes lead to  $e < 1$ ).

The calculated surface temperature variance from Eq. 3.3 compared to the simulated surface temperature variance from the interactive and locked simulations is shown in Fig. 3.12. The temperature variance is shown as a ratio between the interactive and locked simulations. To calculate the surface temperature variance ratio using Eq. 3.3, we calculated Eq. 3.3 twice, one with values from the interactive simulation and once with values from the locked simulation.

Fig. 3.12 demonstrates how well the variance decomposition equation (Eq. 3.3) captures surface temperature variability patterns from the cloud-locking experiments. Comparing the top and bottom panels of Fig. 3.12, it is clear that Eq. 3.3 reproduces surface temperature variance patterns well. Most areas where the simulations indicated cloud-circulation coupling had the most impact on surface temperature variability are the same as where Eq. 3.3 predicted CREs would have the most influence. One notable exception to this is the Arctic, where Eq. 3.3 does not appear to capture the simulated surface temperature variance ratio quite as well. This could be due to the coupling between surface temperature variability and sea-ice variability and how sea-ice variability patterns change with sea-ice thickness (Olonscheck et al., 2019). However, since most other variability patterns are reproduced well, we still considered this equation successful.

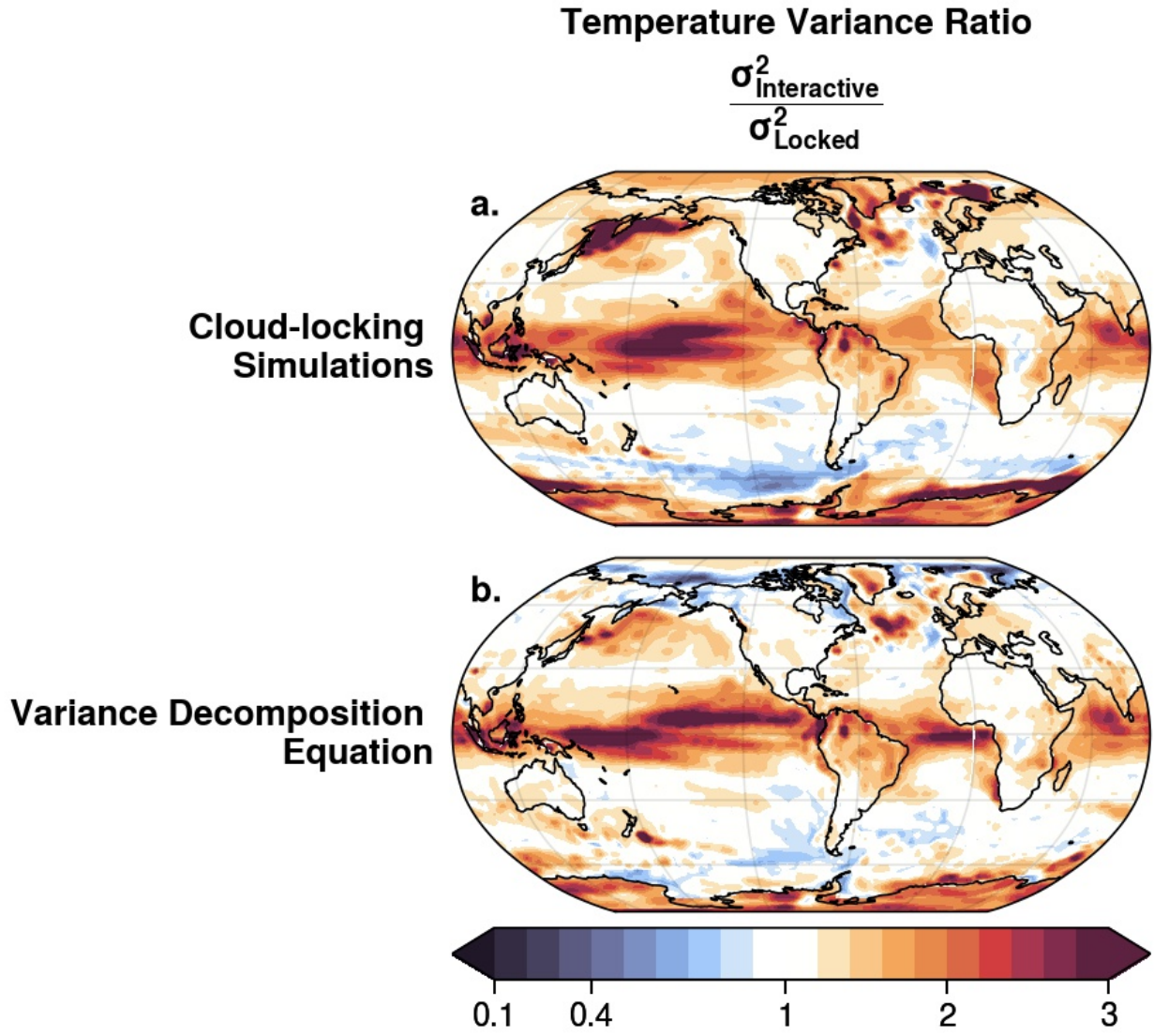


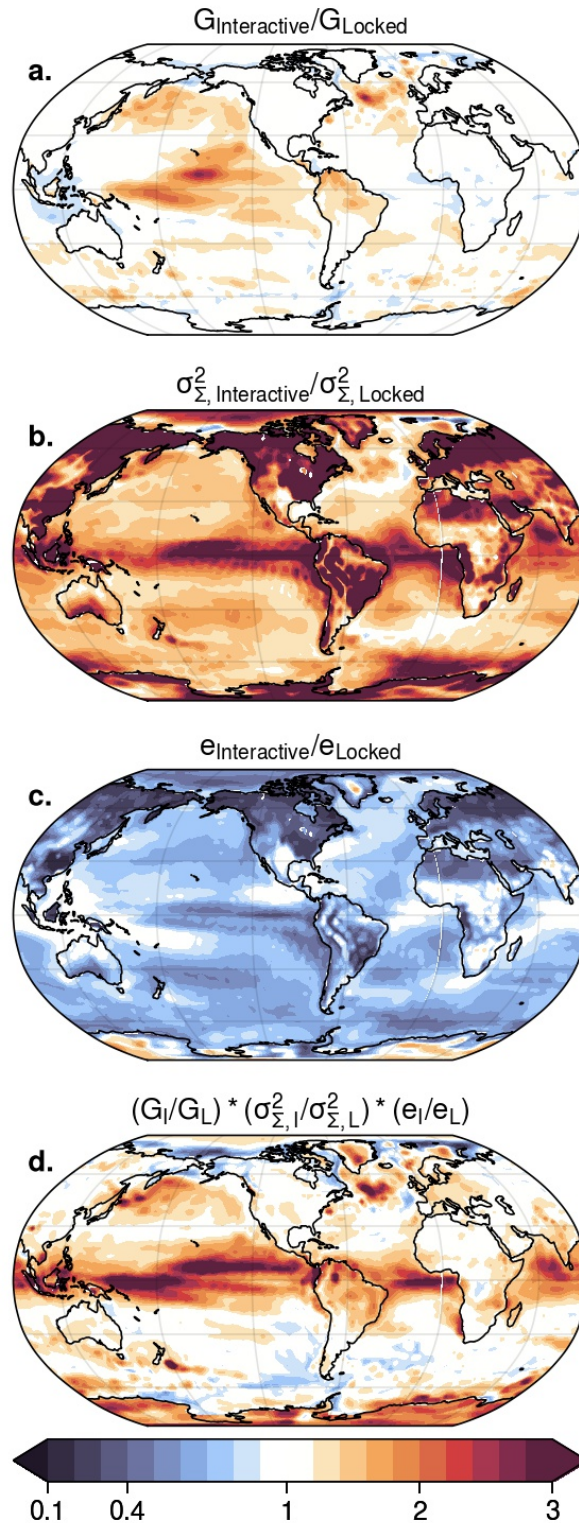
**Figure 3.12:** The ratio of surface temperature variance from the interactive simulation to the locked-cloud simulation for (a) surface temperature variance values from each simulation, and (b) calculated surface temperature variance for each simulation using variance decomposition equation (Eq. 3.3)

This means that this equation can be used to diagnose the mechanisms driving surface temperature variability changes.

To explore the mechanisms behind surface temperature variability changes due to CREs, we first explored how each of the terms in Eq. 3.3 changed from the interactive simulation to the locked simulation. Each of the three terms in Eq. 3.3, calculated as a ratio between the interactive and locked simulations, are shown in Fig. 3.13. As is the case in the tropics (see Li et al., 2020), the increases in surface temperature variance in the extratropics between the interactive and locked runs are dominated by increases in the variances of the fluxes (i.e., increases in the  $\sigma_{\Sigma}^2$  term). The efficiency term ( $e$  term) acts to reduce the effectiveness of the increases in the flux variances due to cross-correlations between the individual fluxes. The transfer term ( $G$  term) acts to modestly enhance the effectiveness of the increases in the flux variances over the oceans since the autocorrelation of the surface temperature field increases in the interactive simulation.

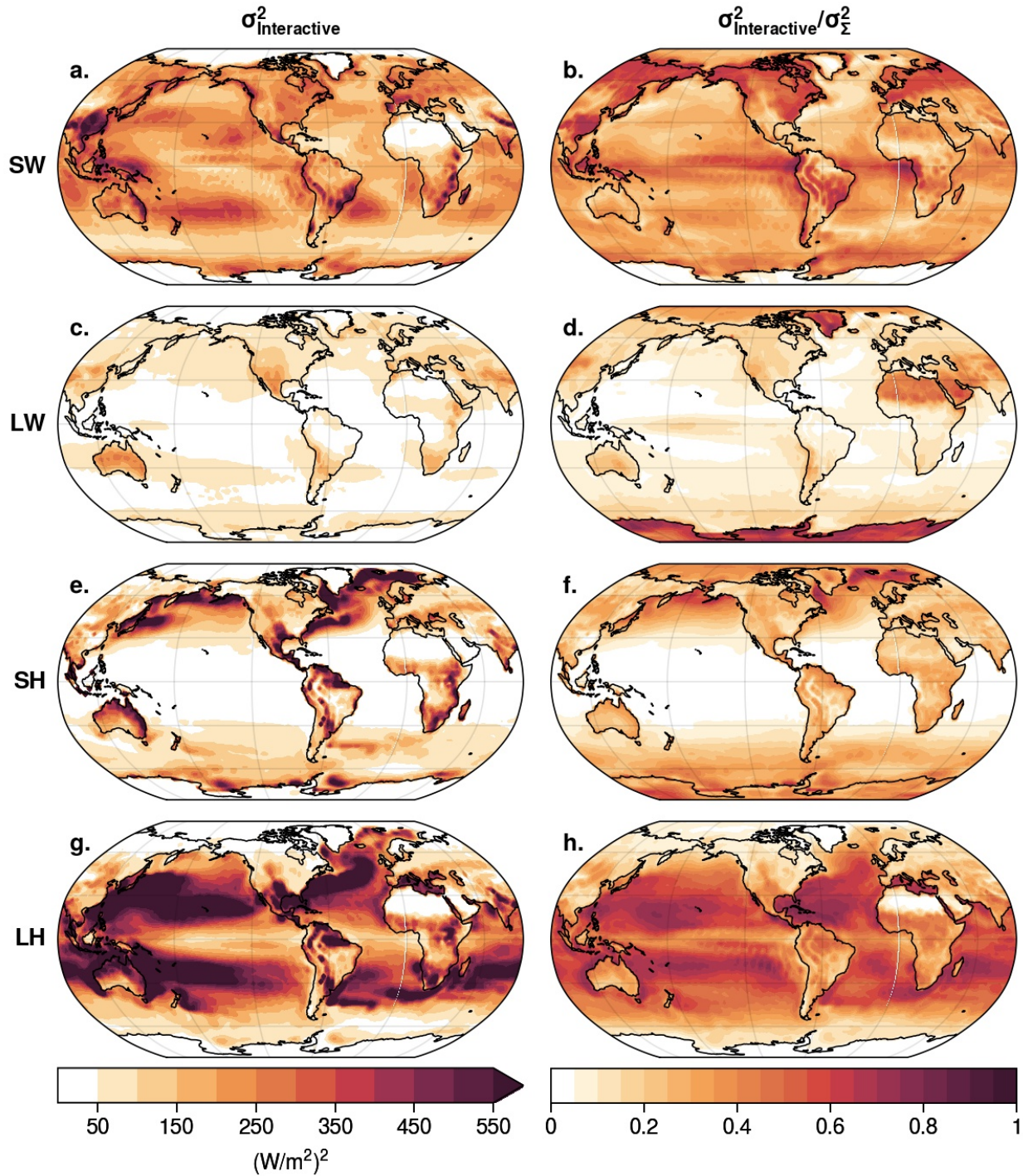
Since the sum of the individual flux variances is the dominating factor in Eq. 3.3, Fig. 3.14 explores the individual surface flux variances and their contribution to the  $\sigma_{\Sigma}^2$  term. The left column shows the climatological-mean surface flux variances in the interactive simulation. In general, the latent, sensible, and shortwave radiative fluxes are the most important for the total variance. The latent heat fluxes are dominant over the subtropical oceans, and the sensible heat fluxes have the largest amplitudes over western boundary current regions, coastal regions, and the periphery of the poles. The radiative flux variances are more spatially amorphous. Looking at the right column of Fig. 3.14, latent heat and shortwave radiative fluxes dominate the  $\sigma_{\Sigma}^2$  term. This indicates that changes in either of these fields would have a greater impact on the total surface flux variability than changes in the longwave radiative or sensible heat flux variability.

Fig. 3.15 explores the changes in the variances of the various individual fluxes between the locked and interactive simulations. The first column shows the climatological-mean surface flux variances in the interactive simulation (reproduced from Fig. 3.14). The second column shows the attendant climatological-mean surface flux variances in the locked simulation. There are clear visual differences in the radiative flux variances between the interactive and locked simulations



**Figure 3.13:** (a-c) The ratio of each term on the right-hand side of Eq. 3.3 calculated for the interactive and locked simulation. (d) Each term on the right-hand side of Eq. 3.3 multiplied together to recreate the surface temperature variance ratio between the interactive and locked simulation.

### Surface Flux Variance and Fractional Contribution to Flux Variance Sum



**Figure 3.14:** Surface energy flux variances: (a,b) surface shortwave radiative flux, (c,d) surface longwave radiative flux, (e,f) surface sensible heat flux, (g,h) surface latent heat. The left column shows the variance for the interactive-cloud simulation. The right column shows the contribution of each individual flux variance to the total surface flux variance of the interactive simulation.

while the differences between simulations for the heat fluxes are less obvious. The right column of this figure illustrates the differences more clearly by showing the ratio of the two simulations for each individual surface flux variance. By far the primary effect of cloud-circulation coupling is to enhance the variance of the shortwave and longwave radiative fluxes (panels c,f). The increases in the shortwave radiative flux variances are prominent across the globe. The increases in the longwave radiative flux variances are relatively weak over ocean areas but comparable to the changes in the shortwave fluxes over terrestrial regions.

Latent and sensible heat flux variance is not substantially impacted by the coupling of clouds to the circulation. In fact, we see a slight decrease in latent heat variance over certain areas of the Southern Ocean due to cloud-circulation coupling. The Southern Ocean has one of the highest cloud cover percentages on Earth with satellite observations showing upwards of 90% steady cloud cover (Mace & Protat, 2018; Mace & Zhang, 2014). This pattern means that the role of shortwave and longwave radiative fluxes in driving changes in SST variability is diminished while latent heat variability becomes a driving factor over that region. This can explain the lack of change or slight decrease in SST variance over areas of the Southern Ocean in the interactive simulation versus the locked simulation (Fig. 3.1c).

The increases in the variances of shortwave radiative fluxes due to cloud-circulation coupling are consistent with the reddening of cloud fraction by the atmospheric flow (Li et al., 2020). That is, low-frequency variability is increased while high-frequency variability is decreased. The mechanism works as follows. In the presence of cloud-circulation coupling, the cloud fraction exhibits power spectra consistent with red noise since the cloud-fields are coupled to large-scale variability in the atmospheric circulation. When the cloud-fields are scrambled and thus decoupled from the circulation, the total variances of cloud fraction are preserved, but the variance is distributed roughly equally across all timescales since there is no persistence in the scrambled cloud-fields. As such when clouds are coupled to the circulation, cloud fraction and shortwave CRE exhibit less variance on very short timescales (e.g. timescales of a few hours) but more variance on low frequency timescales (e.g. timescales longer than a few days).

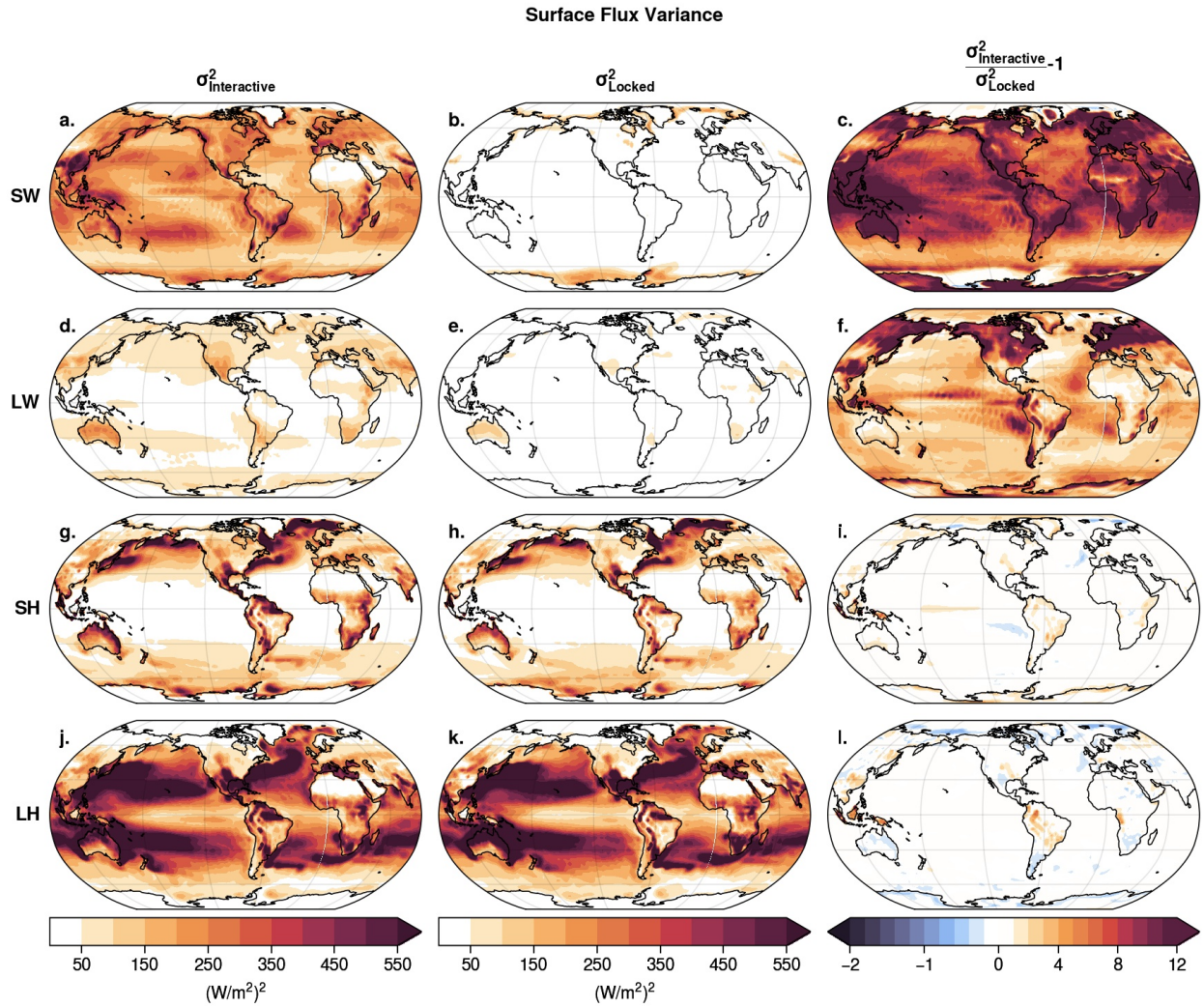


**Figure 3.15:** Surface energy flux variances for the interactive simulation (left column), locked-cloud simulation (middle column), and the fractional change in variance between the two simulations (right column). (a-c) Surface shortwave radiative flux, (d-f) surface longwave radiative flux, (g-i) surface sensible heat flux, and (j-l) surface latent heat flux.

This argument holds for the changes in shortwave radiative flux variance shown in Fig. 3.15c, since the variance of total shortwave flux is dominated by the variance of shortwave CRE. That is, there is minimal variability in the shortwave flux in the locked simulation. The argument also holds for the component of the longwave radiative flux variance that reflects changes in longwave CRE, but it is likely that the changes in the longwave radiative flux variance shown in Fig. 3.15f also arise from changes in temperature variance.

# Chapter 4

## Conclusions

### 4.1 Implications

It is increasingly important to understand the effect that clouds have on not only the mean climate but also its variability. In this work, we used cloud-locking experiments to isolate the impact of cloud-circulation coupling on extratropical climate variability. This experiment involved comparing two simulations: an interactive simulation where clouds are coupled to the atmospheric circulation and a locked simulation where clouds are fully decoupled from the flow. First, we explored the impact of CREs on temperature, geopotential height, and zonal wind variability for multiple levels of the atmosphere. Having found CREs have a robust impact on temperature variability, we explored what timescales upon which surface temperature variability changes were occurring. Finally, we used a simple expression (Eq. 3.3) to explain the driving mechanisms behind changes in surface temperature variance.

Together, the results of this thesis indicate that cloud-circulation coupling has a pronounced effect on climate variability in an Earth System Model across vast regions of the globe. In particular, results show that surface temperature variability is increased due to CREs not only in the tropics (Li et al., 2020; Middlemas et al., 2019; Rädcl et al., 2016), but across much of the extratropics. All of the eight regions explored in this work (North Atlantic, North Pacific, Arctic, North America, Eurasia, Antarctic, and Southern Ocean) showed an increase in area-averaged surface temperature variability due to cloud-circulation coupling. Furthermore, surface temperature variability was found to increase more on low-frequency timescales (multiannual to decadal) versus shorter timescales. In the extratropics, cloud-circulation coupling had the most impact on the North Atlantic and North Pacific, increasing the variability of multiannual to decadal sea-surface temperature (SST) variability by  $\sim 25\%$  and  $\sim 45\%$ , respectively.

In the final part of Chapter 3, CREs were found to dramatically enhance shortwave and long-wave radiative flux variance. This in turn, via the relationship derived in Eq. 3.3, enhanced surface temperature variability. We argued that the same mechanisms that Li et al. (2020) found to enhance tropical SST variability due to CREs, also enhances extratropical surface temperature variability. That is, cloud-circulation coupling acts to redden the cloud fraction by the atmospheric flow, which in turn increases shortwave radiative flux variance on low-frequency timescales and decreases shortwave radiative flux variance on high-frequency timescales. This mechanism thus enhances the contribution of CREs to low-frequency temperature variability.

While previous work has suggested that CREs have a relatively weak effect on extratropical climate variability (e.g. Li et al., 2020; Papavasileiou et al., 2020), this work makes clear the pronounced effect CREs have in the extratropics. These results have important implications for understanding decadal variability of extratropical oceans. Previous research has often focused on air-sea heat fluxes and ocean circulation as the dominant mechanisms of variability (Årthun et al., 2021). Our work suggests that cloud-circulation coupling also makes important contributions to multiannual and decadal patterns of variability such as the Pacific Decadal Oscillation and Atlantic Multidecadal Variability.

## 4.2 Connection to Observations

Since the output from the cloud-locking experiments is model based, it is important to understand if these experiments are a good proxy for the real-world. As such, the variances of the surface fluxes in the interactive simulation were compared to the observed fluxes, as estimated by ERA5 reanalysis (Hersbach et al., 2020) in Fig. 4.1. Comparing the left and right columns of Fig. 4.1, the individual surface flux variances of the interactive simulation bear close resemblance to the flux variances as estimated by ERA5. Thus, in the real-world, cloud-circulation coupling may be viewed as enhancing the variance of low-frequency surface temperature variability by roughly the same amount as in the cloud-locking experiments. In other words, the simulation results of this

work provide a close proxy to the importance of cloud-circulation coupling for climate variability in Earth's climate.

### 4.3 Future Work

This work makes clear the important role of cloud-circulation coupling on low-frequency extratropical climate variability. Thus, we provide a few ways to extend this work. Firstly, these simulations were run only on the MPI Earth System Model. It would be worthwhile to test the robustness of our conclusions by running similar simulations on different global climate models. This would ideally confirm our conclusions and also help to constrain the impact of CREs on extratropical climate variability.

Additionally, previous studies on the impacts of cloud-circulation coupling for the tropical climate have had some disagreement on the specific effect CREs have. Middlemas et al. (2019) argued that CREs enhanced El Niño-Southern Oscillation (ENSO) variability on timescales shorter than 6 years, while Rädel et al. (2016) and Li et al. (2020) argued that CREs enhanced ENSO variability, and more broadly, tropical SST variability across all timescales. Middlemas et al. (2019) had a slightly different locking methodology than the other two studies where in the locked simulation, values of the cloud field were decoupled from the circulation but retained the same autocorrelation. The cloud-locking experiments used in this work had the same locking methodology as Rädel et al. (2016) and Li et al. (2020). As such, it would be interesting to run additional simulations using the same locking methodology as Middlemas et al. (2019) to explore the role of autocorrelation in governing the impact of cloud-circulation coupling on extratropical temperature variability.

Extratropical oceans exhibit considerable decadal variability (Deser & Blackmon, 1993; Deser & Phillips, 2017) and significant recent research has focused on understanding the mechanisms behind this variability (Årthun et al., 2021; Deser et al., 2010; Wills et al., 2021). While the results of this work indicated that cloud-circulation coupling makes significant contributions to decadal variability in the North Atlantic and North Pacific, minimal previous research has been focused on

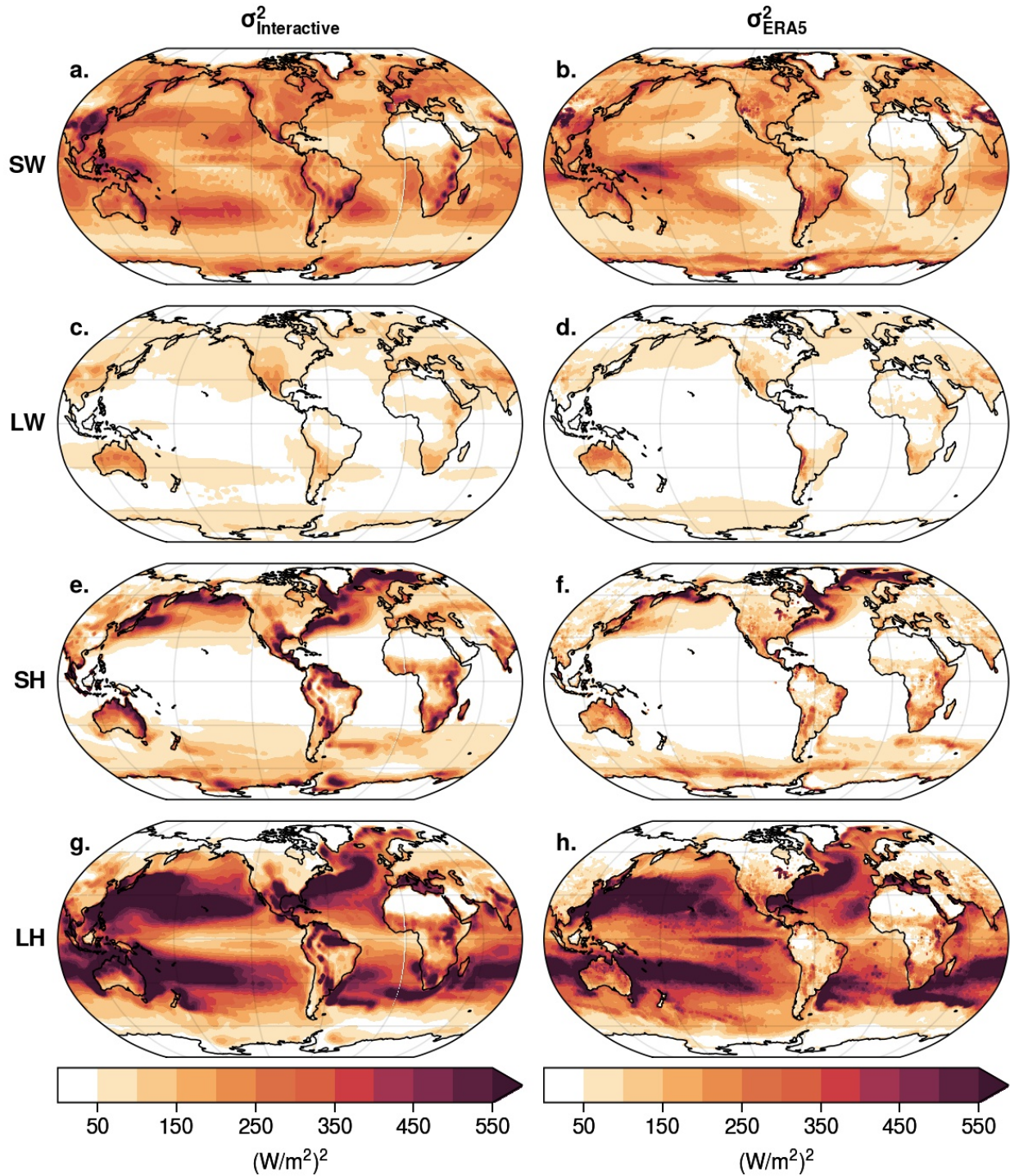


**Figure 4.1:** Surface energy flux variances: (a,b) surface shortwave radiative flux, (c,d) surface longwave radiative flux, (e,f) surface sensible heat flux, (g,h) surface latent heat flux. The left column shows the individual flux variances for the interactive simulation. The right column shows the individual flux variances as estimated by ERA5 reanalysis.

exploring this further. Therefore, it would be a worthwhile expansion on this work to focus on the patterns of variability in the North Atlantic and North Pacific. Specifically constraining the role of clouds in the Pacific Decadal Oscillation and Atlantic Multidecadal Variability would provide important insight on what drives decadal variability in the extratropical oceans.

Furthermore, our results indicate that cloud-circulation coupling acts to enhance surface temperature variability along the periphery of Antarctica as well as the Arctic in the Bering Sea/Labrador Sea regions (see Fig 3.7 a,b and Fig 3.8 a,b). These regions are at the edge of the sea-ice and thus likely see significant sea-ice concentration variability. While the effect of CREs on this sea-ice variability was not explored in this work, a previous study by Olonscheck et al. (2019) found that CREs enhance sea-ice variability at the edges of the sea-ice. Since our results indicated that CREs enhance surface temperature variability at the edge of the sea-ice in the Antarctic, it would be interesting to explore the role of cloud-circulation coupling on Antarctic sea-ice variability.

Lastly, since changes in atmospheric circulation patterns have a dramatic impact on our climate, it is important to understand the implications of this work within the context of climate sensitivity. Using the cloud-locking methodology on CO<sub>2</sub>-forced simulations could help to understand how cloud-circulation coupling will change in the future and the implications of that on other aspects of the future climate.

# Bibliography

- Albern, N., Voigt, A., Buehler, S. A., & Grützun, V. (2018). Robust and Nonrobust Impacts of Atmospheric Cloud-Radiative Interactions on the Tropical Circulation and Its Response to Surface Warming. *Geophysical Research Letters*, *45*(16), 8577–8585.
- Albern, N., Voigt, A., & Pinto, J. G. (2019). Cloud-Radiative Impact on the Regional Responses of the Midlatitude Jet Streams and Storm Tracks to Global Warming. *Journal of Advances in Modeling Earth Systems*, *11*(7), 1940–1958.
- Albern, N., Voigt, A., Thompson, D. W. J., & Pinto, J. G. (2020). The Role of Tropical, Midlatitude, and Polar Cloud-Radiative Changes for the Midlatitude Circulation Response to Global Warming. *Journal of Climate*, *33*(18), 7927–7943.
- Årthun, M., Wills, R. C. J., Johnson, H. L., Chafik, L., & Langehaug, H. R. (2021). Mechanisms of Decadal North Atlantic Climate Variability and Implications for the Recent Cold Anomaly. *Journal of Climate*, *34*(9), 3421–3439.
- Bony, S., Colman, R., Kattsov, V. M., Allan, R. P., Bretherton, C. S., Dufresne, J.-L., Hall, A., Hallegatte, S., Holland, M. M., Ingram, W., Randall, D. A., Soden, B. J., Tselioudis, G., & Webb, M. J. (2006). How Well Do We Understand and Evaluate Climate Change Feedback Processes? *Journal of Climate*, *19*(15), 3445–3482.
- Bony, S., & Dufresne, J.-L. (2005). Marine boundary layer clouds at the heart of tropical cloud feedback uncertainties in climate models. *Geophysical Research Letters*, *32*(20).
- Bony, S., Stevens, B., Frierson, D. M. W., Jakob, C., Kageyama, M., Pincus, R., Shepherd, T. G., Sherwood, S. C., Siebesma, A. P., Sobel, A. H., Watanabe, M., & Webb, M. J. (2015). Clouds, circulation and climate sensitivity. *Nature Geoscience*, *8*(4), 261–268.
- Boucher, O., Randall, D., Artaxo, P., Bretherton, C., Feingold, G., Forster, P., Kerminen, V.-M., Kondo, Y., Liao, H., Lohmann, U., Rasch, P., Satheesh, S. K., Sherwood, S., Stevens, B., & Zhang, X. Y. (2013). Clouds and aerosols. In T. F. Stocker, D. Qin, G.-K. Plattner, M. Tignor, S. K. Allen, J. Doschung, A. Nauels, Y. Xia, V. Bex, & P. M. Midgley (Eds.),

- Climate change 2013: The physical science basis. contribution of working group i to the fifth assessment report of the intergovernmental panel on climate change* (pp. 571–657). Cambridge University Press.
- Cassou, C., Kushnir, Y., Hawkins, E., Pirani, A., Kucharski, F., Kang, I.-S., & Caltabiano, N. (2018). Decadal Climate Variability and Predictability: Challenges and Opportunities. *Bulletin of the American Meteorological Society*, 99(3), 479–490.
- Ceppi, P., & Hartmann, D. L. (2015). Connections Between Clouds, Radiation, and Midlatitude Dynamics: A Review. *Current Climate Change Reports*, 1(2), 94–102.
- Ceppi, P., & Hartmann, D. L. (2016). Clouds and the Atmospheric Circulation Response to Warming. *Journal of Climate*, 29(2), 783–799.
- Deser, C., Alexander, M. A., Xie, S.-P., & Phillips, A. S. (2010). Sea Surface Temperature Variability: Patterns and Mechanisms. *Annual Review of Marine Science*, 2(1), 115–143.
- Deser, C., & Blackmon, M. L. (1993). Surface Climate Variations over the North Atlantic Ocean during Winter: 1900–1989. *Journal of Climate*, 6(9), 1743–1753.
- Deser, C., Phillips, A., Bourdette, V., & Teng, H. (2012). Uncertainty in climate change projections: The role of internal variability. *Climate Dynamics*, 38(3), 527–546.
- Deser, C., & Phillips, A. (2017). An overview of decadal-scale sea surface temperature variability in the observational record. *Past Global Changes Magazine*, 25(1), 2–6.
- Forster, P., Storelvmo, T., Armour, K., Collins, W., Dufresne, J.-L., Frame, D., Lunt, D., Mauritsen, T., Palmer, M., Watanabe, M., Wild, M., & Zhang, H. (2021). The Earth’s Energy Budget, Climate Feedbacks, and Climate Sensitivity [In Press]. In V. Masson-Delmotte, P. Zhai, A. Pirani, S. Connors, C. Péan, S. Berger, N. Caud, Y. Chen, L. Goldfarb, M. Gomis, M. Huang, K. Leitzell, E. Lonnoy, J. Matthews, T. Maycock, T. Waterfield, O. Yelekçi, R. Yu, & B. Zhou (Eds.), *Climate Change 2021: The Physical Science Basis. Contribution of Working Group I to the Sixth Assessment Report of the Intergovernmental Panel on Climate Change*. Cambridge University Press.

- Grise, K. M., Medeiros, B., Benedict, J. J., & Olson, J. G. (2019). Investigating the Influence of Cloud Radiative Effects on the Extratropical Storm Tracks. *Geophysical Research Letters*, *46*(13), 7700–7707.
- Hartmann, D. L. (2016). Chapter 4 - The Energy Balance of the Surface. In D. L. Hartmann (Ed.), *Global Physical Climatology (Second Edition)* (pp. 95–130). Elsevier.
- Hersbach, H., Bell, B., Berrisford, P., Hirahara, S., Horányi, A., Muñoz-Sabater, J., Nicolas, J., Peubey, C., Radu, R., Schepers, D., Simmons, A., Soci, C., Abdalla, S., Abellan, X., Balsamo, G., Bechtold, P., Biavati, G., Bidlot, J., Bonavita, M., . . . Thépaut, J.-N. (2020). The ERA5 global reanalysis. *Quarterly Journal of the Royal Meteorological Society*, *146*(730), 1999–2049.
- Hunt, B. G. (1978). On the general circulation of the atmosphere without clouds. *Quarterly Journal of the Royal Meteorological Society*, *104*(439), 91–102.
- Li, Y., Thompson, D. W. J., & Bony, S. (2015). The Influence of Atmospheric Cloud Radiative Effects on the Large-Scale Atmospheric Circulation. *Journal of Climate*, *28*(18), 7263–7278.
- Li, Y., Thompson, D. W. J., Huang, Y., & Zhang, M. (2014). Observed linkages between the northern annular mode/North Atlantic Oscillation, cloud incidence, and cloud radiative forcing. *Geophysical Research Letters*, *41*(5), 1681–1688.
- Li, Y., Thompson, D. W. J., & Olonscheck, D. (2020). A Basic Effect of Cloud Radiative Effects on Tropical Sea Surface Temperature Variability. *Journal of Climate*, *33*(10), 4333–4346.
- Loeb, N. G., Doelling, D. R., Wang, H., Su, W., Nguyen, C., Corbett, J. G., Liang, L., Mitrescu, C., Rose, F. G., & Kato, S. (2018). Clouds and the Earth’s Radiant Energy System (CERES) Energy Balanced and Filled (EBAF) Top-of-Atmosphere (TOA) Edition-4.0 Data Product. *Journal of Climate*, *31*(2), 895–918.
- Mace, G. G., & Protat, A. (2018). Clouds over the Southern Ocean as Observed from the R/V Investigator during CAPRICORN. Part I: Cloud Occurrence and Phase Partitioning. *Journal of Applied Meteorology and Climatology*, *57*(8), 1783–1803.

- Mace, G. G., & Zhang, Q. (2014). The CloudSat radar-lidar geometrical profile product (RL-GeoProf): Updates, improvements, and selected results. *Journal of Geophysical Research: Atmospheres*, *119*(15), 9441–9462.
- Mauritsen, T., Bader, J., Becker, T., Behrens, J., Bittner, M., Brokopf, R., Brovkin, V., Claussen, M., Crueger, T., Esch, M., Fast, I., Fiedler, S., Fläschner, D., Gayler, V., Giorgetta, M., Goll, D. S., Haak, H., Hagemann, S., Hedemann, C., . . . Roeckner, E. (2019). Developments in the MPI-M Earth System Model version 1.2 (MPI-ESM1.2) and Its Response to Increasing CO<sub>2</sub>. *Journal of Advances in Modeling Earth Systems*, *11*(4), 998–1038.
- Middlemas, E. A., Clement, A. C., Medeiros, B., & Kirtman, B. (2019). Cloud Radiative Feedbacks and El Niño–Southern Oscillation. *Journal of Climate*, *32*(15), 4661–4680.
- Olonscheck, D., Mauritsen, T., & Notz, D. (2019). Arctic sea-ice variability is primarily driven by atmospheric temperature fluctuations. *Nature Geoscience*, *12*(6), 430–434.
- Papavasileiou, G., Voigt, A., & Knippertz, P. (2020). The role of observed cloud-radiative anomalies for the dynamics of the North Atlantic Oscillation on synoptic time-scales. *Quarterly Journal of the Royal Meteorological Society*, *146*(729), 1822–1841.
- Rädel, G., Mauritsen, T., Stevens, B., Dommenges, D., Matei, D., Bellomo, K., & Clement, A. (2016). Amplification of El Niño by cloud longwave coupling to atmospheric circulation. *Nature Geoscience*, *9*(2), 106–110.
- Ramanathan, V. (1987). The role of earth radiation budget studies in climate and general circulation research. *Journal of Geophysical Research: Atmospheres*, *92*(D4), 4075–4095.
- Ramanathan, V., Cess, R. D., Harrison, E. F., Minnis, P., Barkstrom, B. R., Ahmad, E., & Hartmann, D. (1989). Cloud-Radiative Forcing and Climate: Results from the Earth Radiation Budget Experiment. *Science*, *243*(4887), 57–63.
- Schäfer, S. A. K., & Voigt, A. (2018). Radiation Weakens Idealized Midlatitude Cyclones. *Geophysical Research Letters*, *45*(6), 2833–2841.
- Sherwood, S. C., Webb, M. J., Annan, J. D., Armour, K. C., Forster, P. M., Hargreaves, J. C., Hegerl, G., Klein, S. A., Marvel, K. D., Rohling, E. J., Watanabe, M., Andrews, T., Bra-

- connot, P., Bretherton, C. S., Foster, G. L., Hausfather, Z., von der Heydt, A. S., Knutti, R., Mauritsen, T., ... Zelinka, M. D. (2020). An Assessment of Earth's Climate Sensitivity Using Multiple Lines of Evidence. *Reviews of Geophysics*, 58(4), e2019RG000678.
- Slingo, A., & Slingo, J. M. (1988). The response of a general circulation model to cloud longwave radiative forcing. I: Introduction and initial experiments. *Quarterly Journal of the Royal Meteorological Society*, 114(482), 1027–1062.
- Stephens, G. L., Li, J., Wild, M., Clayson, C. A., Loeb, N., Kato, S., L'Ecuyer, T., Stackhouse, P. W., Lebsock, M., & Andrews, T. (2012). An update on Earth's energy balance in light of the latest global observations. *Nature Geoscience*, 5(10), 691–696.
- Stevens, B., Bony, S., & Webb, M. (2012). Clouds on-Off Klimate Intercomparison Experiment (cookie).
- Voigt, A., & Albern, N. (2019). No Cookie for Climate Change. *Geophysical Research Letters*, 46(24), 14751–14761.
- Voigt, A., Albern, N., Ceppi, P., Grise, K., Li, Y., & Medeiros, B. (2021). Clouds, radiation, and atmospheric circulation in the present-day climate and under climate change. *WIREs Climate Change*, 12(2), e694.
- Voigt, A., & Shaw, T. A. (2015). Circulation response to warming shaped by radiative changes of clouds and water vapour. *Nature Geoscience*, 8(2), 102–106.
- Voigt, A., & Shaw, T. A. (2016). Impact of Regional Atmospheric Cloud Radiative Changes on Shifts of the Extratropical Jet Stream in Response to Global Warming. *Journal of Climate*, 29(23), 8399–8421.
- Wills, R. C. J., Johnson, H. L., Chafik, O., & Langehaug, H. R. (2021). Mechanisms of Decadal North Atlantic Climate Variability and Implications for the Recent Cold Anomaly. *Journal of Climate*, 34, 19.
- Yu, B., & Boer, G. J. (2006). The variance of sea surface temperature and projected changes with global warming. *Climate Dynamics*, 26(7), 801–821.

Zelinka, M. D., & Hartmann, D. L. (2010). Why is longwave cloud feedback positive? *Journal of Geophysical Research: Atmospheres*, 115(D16).

# Appendix A

## Surface Temperature Variance Decomposition

Starting from surface energy balance in Eq. 3.1, the derivation of Eq. 3.3 is outlined following Yu and Boer (2006) and Li et al. (2020). First taking the centered difference of Eq. 3.1, we get:

$$C \frac{T(t + \Delta t) - T(t - \Delta t)}{2\Delta t} = Q_{SW} + Q_{LW} + Q_{SH} + Q_{LH}. \quad (\text{A.1})$$

Next, we square this equation and take the time average (denoted by an overline). The LHS of the resulting equation is:

$$\frac{C^2}{2(\Delta t)^2} (\overline{T(t)^2} - \overline{T(t - \Delta t)T(t + \Delta t)}). \quad (\text{A.2})$$

The lag-2 autocorrelation of anomalous surface temperature is defined as

$$r_2 = \frac{\overline{T(t + \Delta t)T(t - \Delta t)}}{\overline{T(t)^2}}, \quad (\text{A.3})$$

so Eq. A.2 can be simplified to

$$\frac{C^2(1 - r_2)}{2(\Delta t)^2} \sigma_T^2 \quad (\text{A.4})$$

where  $\sigma_T^2$  is the monthly-mean surface temperature variance. Now the RHS after squaring and taking the time average of Eq. A.1. is

$$\sigma_\Sigma^2 + 2 \sum cov(Q_i, Q_j), \quad (\text{A.5})$$

where  $\sigma_\Sigma^2$  is equal to the sum of each individual surface flux variance:  $\sigma_\Sigma^2 = \sigma_{SW}^2 + \sigma_{LW}^2 + \sigma_{SH}^2 + \sigma_{LH}^2$  and  $\Sigma cov(Q_i, Q_j)$  is the covariance between each surface flux. Setting the LHS (Eq. A.4) and the RHS (Eq. A.5) equal to each other and then solving for the temperature variance we arrive at:

$$\sigma_T^2 = \frac{2(\Delta t)^2}{C^2(1 - r_2)} \left( \sigma_\Sigma^2 + 2 \sum cov(Q_i, Q_j) \right). \quad (\text{A.6})$$

We can simplify this equation further by defining  $G = \frac{2(\Delta t)^2}{C^2(1-r_2)}$  and  $e = 1 + \frac{2\Sigma cov(Q_i, Q_j)}{\sigma_\Sigma^2}$ . The resulting equation is

$$\sigma_T^2 = G\sigma_\Sigma^2 e, \tag{A.7}$$

which is equivalent to Eq. 3.3.